Modal Analysis of Rigid Microphone Arrays using Boundary Elements

Master thesis

Fabio Kaiser

Supervisor: Dr. Franz Zotter
Co-Supervisor: Dr. Filippo Fazi

Assessor: o. Univ.-Prof. Mag. DI. Dr. Robert Höldrich







Institute of Electronic Music and Acoustics
University of Music and Performing Arts, Graz, Austria
June 2012

Abstract

This thesis deals with compact rigid microphone arrays and their acoustic modal representation for sound field reconstruction and beamforming. A method for obtaining surface modes of arbitrarily shaped rigid microphone arrays based on the boundary element method (BEM) and the singular value decomposition (SVD) is introduced and an analysis of spherical and cylindrical arrays is presented. The modal functions are found to be frequency dependent except for frequencies below $kr \approx 1$. This indicates that a simplification of the array signal processing can be applied for low frequencies. Further, the spatial resolution properties of different rigid spherical and cylindrical array shapes were analyzed. The different configurations simulated using the BEM were found to have similar vertical and horizontal resolution.

Keywords: acoustic radiation modes, boundary element method, microphone arrays, scattering, singular value decomposition, modal array processing, array modes.

Zusammenfassung

Diese Arbeit beschäftigt sich mit kompakten und festen Mikrofonanordnugnen und deren akustischer modaler Beschreibung. Eine Methode zur Berechnung von Oberflächenmoden, die auf der Singulärwertzerlegung und der Randelementmethode basiert, wird vorgestellt, und eine Analyse von Kugel- und Zylinderanordnungen wird gezeigt. Die modalen Funktionen sind frequenzabhängig außer für Frequenzen unter $kr \approx 1$. Dies weist darauf hin, dass die Array-Signalverarbeitung für tiefe Frequenzen vereinfacht werden kann. Weiters wurde die räumliche Auflösung von verschiedenen Kugel- und Zylinderanordnungen analysiert und es wurde gezeigt, dass diese Anordnungen sich nicht essentiell unterscheiden in ihrer Fähigkeit, verschiedene Schalleinfallsrichtungen zu diskriminieren.

Acknowledgements

I want to thank my family for their support and caring throughout all these years of study. My thanks also belongs to Dr. Alois Sontacchi for his support in making several experiences in my study possible. Special thanks to my supervisor, Dr. Franz Zotter, who definitely spent too much time on the phone with me and taught me many things. Especially, I want to mention his corrections and comments on my writing. He increased the quality of this thesis substantially. Further, I want to thank my second supervisor, Dr. Filippo Fazi, who gave me insights into the field of acoustics throughout long discussions and warmly welcomed me in Southampton.

This work has been undertaken partly at the I Institute of Electronic Music and Acoustics (IEM), Graz, Austria, and partly at the Institute of Sound and Vibration Research (ISVR), Southampton, England. Both institutions were incredible places to be at as a student.

Contents

1 Introduction **7**
1.1 This Work 10

2 Analytical Description of Sound Fields **11**
2.1 Helmholtz Equation 11
2.2 Boundary Conditions 12
2.2.1 Interior and Exterior Solutions 13
2.2.2 Sommerfeld Radiation Condition 14
2.3 Solutions of the Elementary Inhomogeneous Problem 15
2.3.1 Green's Function 15
2.3.2 Helmholtz Integral Equation 16
2.4 Elementary Solutions of the Homogeneous Problem 17
2.4.1 Cylindrical Coordinates 18
2.4.2 Spherical Coordinates 20
2.5 Summary 21

3 Boundary Element Method **22**
3.1 Basics 22
3.1.1 Existence and Uniquness 23
3.2 Numerical Implementation 24
3.3 Axisymmetric Formulation 26
3.4 Summary 27

4 Modal Analysis of Free-Field Scatterers **28**
4.1 The Scattering Operator 29
4.1.1 Spherical Source Distribution 31
4.2 Scattering Matrix via BEM 33
4.2.1 SVD of the Scattering Matrix 34
4.2.2 Joint SVD 35
4.3 Simulation Results 36
4.3.1 Sampling of the Generator 37

4.3.2 Sphere 37
4.3.3 Cylinder 38
4.4 Discussion 47

5 Spatial Resolution of Cylindrical Microphone Arrays 49
5.1 Introduction 49
5.2 Analysis of Spatial Resolution 50
5.3 Simulation Results 52
5.4 Discussion 53

6 Conclusions 57

Appendices

A Fourier Analysis 59
A.1 Fourier Series 59
A.2 Generalized Fourier Series 59
A.3 Fourier Transform 61

B Special Functions 63
B.1 Bessel Functions 63
B.2 Associated Legendre Functions 63
B.3 Spherical Harmonics 65

C Beamforming as an Inverse Problem 67

D Modal Analysis of Free-Field Radiators 69
D.1 The Radiation Problem 69
D.1.1 Singular Functions of the Radiation Operator 70
D.1.2 Neumann Green's Function Matrix 71
D.1.3 SVD of Neumann Green's Function Matrix 72
D.2 Radiation Modes for Varying Scalings 72

Bibliography 74

Chapter 1

Introduction

Microphone arrays are used for the analysis of acoustic scenes (acoustic scene analysis) where several sound sources can either be of interest or disturbing (Fig. 1.1). The engineering task is to extract information out of a sound field, e.g., the location of sound sources or the number of sound sources. Further, the aim could be to focus on specific sound sources and to try to extract the source sound field and suppress sound sources from other locations (beamforming, beamsteering). These techniques are of interest for acoustic surveillance systems and speech recognition- and telecommunication systems. Other applications of microphone arrays are 3D sound recording and room acoustic analysis.

Sound Field Analysis by Microphone Arrays

When using acoustic models to predict sound propagation [MF53] it is necessary to estimate the parameters of the model. Microphone arrays state the practical method to acquire boundary values with which the model parameters can be solved for [GG06]. The measured signals of microphone arrays form a spatial function in frequency domain and therefore a decomposition is achieved by projection on orthogonal spatial basis functions. Any further processing is done using the coefficients of the decomposition instead of the microphone signals themselves and if the set of basis functions is complete, a reconstruction is possible without loss. This paradigm of microphone array signal processing and acoustic modeling is based on generalized Fourier transforms [Wil99, Teu07]. The transformation considerably simplifies the necessary signal processing for tasks like localization of sound sources or beamforming. Related applications are Near-Field Acoustical Holography [Wil99, Sar90, VW04], sound field reconstruction [Faz10] and active control of sound [NE93, EJ93].

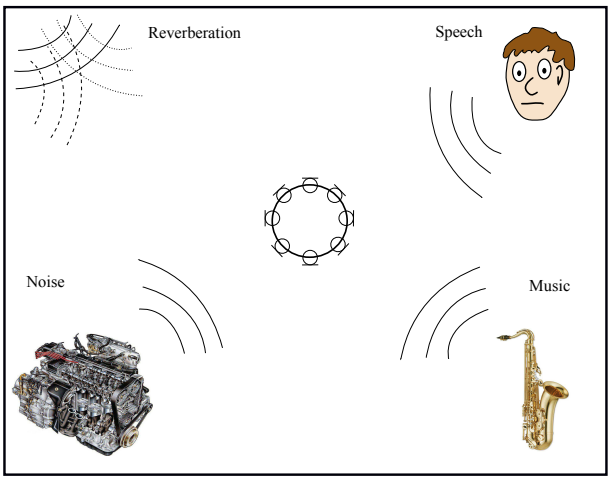


Figure 1.1: Acoustic problem scenario where several sound source are either of interest or should be suppressed in the recording.

Solution methods and solutions for acoustic problems are well documented in the literature [MF53, AW05, AS64]. Of interest in the context of this work is the *separation of variables* of the Helmholtz equation and the solutions of the resulting ordinary differential equations. The separation of the Helmholtz equation and the resulting basis functions are given in different separable coordinate systems, e.g., the cylindrical and the spherical coordinate system [Wei12]. However, these solutions are not always of practical relevance or applicability, e.g., in the case of a finite-length cylinder [Teu07]. In some cases, geometries which do not correspond to an orthogonal coordinate systems can be of interest but the corresponding functions for the decomposition are not known. Therefore, methods have been proposed to compute basis functions for unconventional geometries [Bor90, Sar91]. This work deals with the problem of obtaining such functions.

Generalized Modal Beamformer

The process to extract sound of a certain area in space only is called beamforming and beamforming based on a generalized Fourier series using orthogonal functions or "modal functions"[1] is called modal beamforming [Teu07]. Spherical microphone arrays and the corresponding spherical modal beamformer are well-described [ME02, AW02, Raf05]. The hardware requirements and the practical complexity of spherical microphone arrays is high and as the

[1]The modal functions in this context mean vibration modes of the surface of a body and have to be clearly differentiated from structural modes.

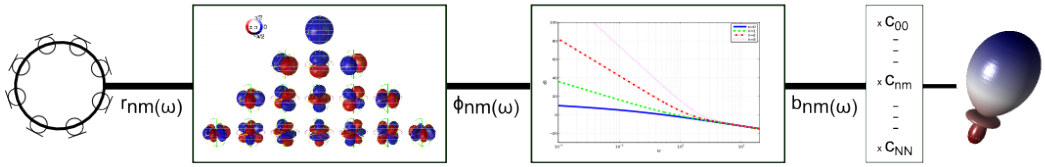


Figure 1.2: Block scheme of the processing steps of a spherical microphone array. The measured frequency domain signals are projected on the spherical harmonics, then equalized and then the a beam is formed using specific weigths.

resolution of full 3D space may be redundant, alternative array shapes have been investigated. Circular arrays state an evident alternative [Mey01, TK06] but also a hemispherical array has been proposed [LD05].

A modal beamformer relies on the knowledge of orthogonal modal functions. As mentioned, these functions are well-described for simple array shape like the sphere, but other shapes have no such simple description. Fig. 1.2 plots a block-diagram of the modal array signal processing necessary to achieve modal beamforming using a spherical microphone array. The question is if we can find a similar processing scheme for other, unconventional array shapes.

Spatial Resolution

The modal sound field analysis approach relies on the modal functions to be a complete set of orthogonal functions. Completeness requires an infinite set or at least a very large number of modal functions [Kre06]. However, practical microphone arrays cannot be realized having a continuous sound pressure sensitive surface and therefore systems having a finite number of degrees of freedom can be achieved only. Due to the discrete sampling of space it is impossible to retrieve an infinite number of modes, and spatial aliasing effects, equivalent to time aliasing, will occur [RWB07]. This means that a modal beamformer cannot resolve space with infinite precision. The shape of the beam, and therefore the spatial resolution is determined by the number of modal functions used. The more functions are used, the higher the resolution. However, specific shapes and configurations of microphone arrays might support the resolution of certain areas in space while the resolution of other areas is reduced. Also this will be addressed in the thesis.

1.1 This Work

This work investigates the modal representation of unconventional microphone array shapes and their spatial resolution properties. A goal is to apply a modal decomposition over the measurement surface separated into frequency independent functions and functions that are dependent on the ratio of wavelength to body dimensions. The case of a spherical microphone array is well described and will be used as a reference case. However, the modal processing for unconventional array shapes has not been described in the same detail in the available literature. The main research question raised in this work are:

- Can modal functions for alternative array shapes be found? Do they behave similar to the functions of the spherical case in terms of frequency independence? Are they real-valued?
- How do the spatial resolution properties change when the array shape is changed? Can certain areas in space be emphasized over others?

The investigations presented focus on the acoustic front-end of the whole engineering chain of microphone arrays.

The thesis is structured as follows. In chapter 2 the basic theory of analytical acoustics is reviewed and the tools necessary for later chapters are presented. Chapter 3 introduces the boundary element method (BEM) which offers a numerical treatment of radiation and scattering problems in nearly arbitrary geometries. The reader familiar with analytical and numerical concepts of acoustics can jump right to chapter 4, which is the main part of this thesis. It introduces a method to compute modal functions of general scatterers based on the BEM and the singular value decomposition (SVD). The method is similar to other methods of literature but it differs in that the scattering problem is regarded more closely in contrast to the radiation problem. In principal, also array modes of open microphone arrays can be computed using the SVD but this is not regarded here. Finally, chapter 5 introduces a method to describe the spatial resolution of general microphone arrays. The method is based on the determinant of a correlation matrix of the array response to two incoming plane wave field of different incidence angle. In both chapters 4 and 5 cylindrical arrays of different dimension are exemplified and the simulation results are compared to spherical arrays. In appendix A the Fourier analysis is reviewed and in appendix B some special function, e.g. the spherical harmonics are defined. App. C explains the inverse problem a beamforming task states and App. D reviews the method for obtaining modal functions based on the Green's function matrix.

Chapter 2

Analytical Description of Sound Fields

The mathematical model of sound propagation is given by the wave equation[1] which describes the relation of sound pressure in time and space. Solutions for radiation and scattering problems have been given in the literature [MF53, MI86, Wil99]. In many cases it is sufficient and easier to describe time-harmonic sound propagation only. This leads to the reduced wave equation, also called the Helmholtz equation.

The coming sections show the mathematical formulations of linear and lossless wave propagation which are used as basics throughout this thesis.

2.1 Helmholtz Equation

The Helmholtz equation is named after Hermann von Helmholtz[2]. It describes time-harmonic processes, i.e., $p(\boldsymbol{x}, t) = Re\{p(\boldsymbol{x}, \omega)e^{i\omega t}\}$, and it is equivalent to the Fourier transform of the wave equation. The inhomogeneous Helmholtz equation is written as

$$(\Delta + k^2)p(\boldsymbol{x}, \omega) = -q(\boldsymbol{x}, \omega) \ , \tag{2.1}$$

where $k = \frac{\omega}{c} = \frac{2\pi}{\lambda}$ is the wavenumber, $\omega = 2\pi f$ and f is the frequency, c is the speed of sound, p is the sound pressure, q is a source term and Δ is the Laplacian operator, in cartesian coordinates defined by

[1] For a detailed derivation of the wave equation see [MF53, Ch. 6]

[2] Hermann von Helmholtz (1821-1894), German physician and physicist.

$$\Delta \equiv \frac{\partial^2}{\partial x^2} + \frac{\partial^2}{\partial y^2} + \frac{\partial^2}{\partial z^2} \,. \tag{2.2}$$

A further important equation is the Euler equation given by

$$\mathrm{i}\omega\rho_0 \, \vec{v}(\boldsymbol{x}, \omega) = \nabla p(\boldsymbol{x}, \omega) \,. \tag{2.3}$$

where ρ_0 is the air density, $\vec{v}$ is the particle velocity and ∇ is the gradient defined by

$$\nabla \equiv \frac{\partial}{\partial x}\vec{e}_x + \frac{\partial}{\partial y}\vec{e}_y + \frac{\partial}{\partial z}\vec{e}_z \,, \tag{2.4}$$

where $\vec{e}_x, \vec{e}_y, \vec{e}_z$ are the standard unit vectors. Euler's equation originates from Newtons second law, $\vec{F} = m\vec{a}$, and relates the change of sound pressure in space to the acceleration of particles. The dependence on ω will be dropped for the rest of this thesis, to simplify the notation.

The Helmholtz equation is a partial differential equation (PDE). In order to ensure existence and uniqueness of solutions, boundary conditions have to be defined. The inhomogeneous problem stated by Eq. 2.1 is solved under physical conditions by two different approaches. One approach is to use elementary solutions which solves an inhomogeneous problem excited at one point in space. More general inhomogeneous problems are solved by superimposing this elementary solution by shifting and weighting in space. This is based on the theory of Green's function [MF53, CK98, GG06, Wil99] and will be shortly reviewed in section 2.3. Another approach is to use elementary solutions for the homogeneous problem that can be found for dedicated coordinate systems. Combinations of different elementary solutions fulfill boundary conditions that are easily described in the respective coordinate system and can be used to solve an inhomogeneous problem. This approach is based on the generalized Fourier transforms [MF53, Wil99, GG06] and will be introduced in section 2.4.

2.2 Boundary Conditions

As it is the case with every kind of PDE, also the wave equation can only be solved subject to certain boundary conditions and it will be seen that a boundary condition forcing the normal particle velocity to zero is of interest in this work. Basically there are three types of boundary conditions. Either the functions of interest is directly prescribed or its derivative or a mix of

both. In acoustics, a specification of the sound pressure $p(\boldsymbol{x})$ leads to so called *Dirichlet* boundary conditions,

$$p(\boldsymbol{x}) = \bar{p}\,, \tag{2.5}$$

where $\boldsymbol{x} \in S$ with S being a boundary surface and $\bar{p}$ indicates a known value, e.g. $\bar{p} = 0$ which corresponds to a homogeneous Dirichlet condition (pressure release case).

If the normal derivative of the function is prescribed it is called a *Neumann* boundary condition

$$\frac{\partial p(\boldsymbol{x})}{\partial \mathbf{n}} = \bar{p}_{\mathrm{n}}\,, \tag{2.6}$$

and if the known or measured value $\bar{p}_{\mathrm{n}} = 0$ it corresponds to a homogeneous Neumann condition, (rigid case).

The third case applies when a mix of Neumann and Dirichlet conditions are prescribed

$$\alpha\; p(\boldsymbol{x}) + \beta\; v_{\mathrm{n}}(\boldsymbol{x}) = \gamma \tag{2.7}$$

where α, β, γ are arbitrary complex constants and v_{n} is the normal particle velocity. This type of condition is called an impedance boundary conditions or Robin boundary conditions [Wei12]. If we reorder for the velocity, Eq. 2.7 is written as

$$v_{\mathrm{n}}(\boldsymbol{x}) = -\frac{\alpha}{\beta}\; p(\boldsymbol{x}) + \frac{\gamma}{\beta} \tag{2.8}$$

where the left term on the right side $\frac{\alpha}{\beta}$ is an acoustic admittance Y and the right term is a forced or prescribed velocity v_s

$$v_{\mathrm{n}}(\boldsymbol{x}) = -Y\; p(\boldsymbol{x}) + v_{\mathbf{s}}(\boldsymbol{x})\;. \tag{2.9}$$

In this equation, $v_{\mathbf{s}}$ is the velocity of vibration of a structure and $Yp(\boldsymbol{x})$ the velocity boundary layer of the fluid in connection to the structure [KP11] [MH99]. A vibrating structure having absorbing material stitched to it corresponds to the case when Y is non-zero.

2.2.1 Interior and Exterior Solutions

Solutions of the Helmholtz equation found using boundary conditions are often described as regular or singular solutions. This is done by defining two regions in space, the interior and the exterior domain or a mix (see Fig. 2.1). Solutions for the interior region have to be finite and no singularities

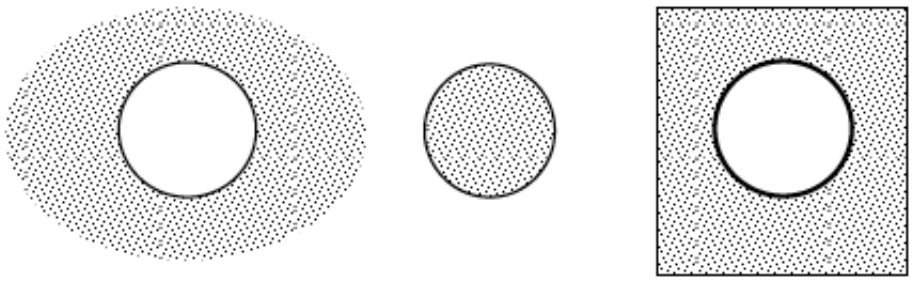


Figure 2.1: Exterior, interior and a mixed (or combined) problem [Wil99].

are allowed. Therefore they are called, regular solutions. Solutions for the exterior region just have to satisfy the Sommerfeld radiation condition, which assures that no sources exist in infinity. Therefore they are called singular solutions.

The values on the boundary separating the regions can be used to solve the acoustic model and compute the sound field in the source-free region. The boundary values are either known, numerically calculated or measured. In this way a direct solution of the PDE with its inhomogenuity is circumvented and an indirect approach where the boundary values determine the sound field is taken. For a more detailed description of boundary value problems see [MF53, Ch. 6],[CK91, Ch. 3] and [Zot09].

2.2.2 Sommerfeld Radiation Condition

For exterior problems, where the domain extends to infinity, the Sommerfeld radiation condition has to be fulfilled as a boundary condition

$$\lim_{R\to\infty} \left[R \left| \frac{\partial p(\boldsymbol{x})}{\partial R} - \mathrm{i}kp(\boldsymbol{x}) \right|\right] = 0 \tag{2.10}$$

where R is the radius of a sphere which circumscribes the radiating or scattering object [Som92]. It ensures that the infinitely extended radiating/scattered sound field is free from components that are not bounded in space and therefore not caused by the source/scatterer of finite energy and size.

2.3 Solutions of the Elementary Inhomogeneous Problem

The solved inhomogeneous Helmholtz equation can be reformulated as an integral with the elementary solution, the Green's functions, as its kernel. Given the inhomogenous problem stated in Eq. 2.1 and knowing the free-field Green's function $G(\boldsymbol{x}|\boldsymbol{x}_0)$, the solution is given by

$$p(\boldsymbol{x}) = \int_V q(\boldsymbol{x}_0)\, G(\boldsymbol{x}|\boldsymbol{x}_0)\, \mathrm{d}V\,, \tag{2.11}$$

where V indicates a volume integral [Wil99, sec. 8.6].

Using Green's third integral identity yields a well known boundary integral where the sound pressure is measured or given on a boundary surrounding or excluding the sound sources. This boundary integral is called the Helmholtz integral equation (HIE).

2.3.1 Green's Function

A Green's function is the elementary solution to the inhomogeneous Helmholtz equation subject to possible additional boundary conditions. A special case is the free-field Green's function, which is the solution in infinite domain of the set of equations:

$$\begin{cases} (\Delta + k^2) G(\boldsymbol{x}|\boldsymbol{x}_0) = -\delta(\boldsymbol{x} - \boldsymbol{x}_0)\,, \\ \lim\limits_{r\to\infty} G(\boldsymbol{x}|\boldsymbol{x}_0) = 0\,, \end{cases} \tag{2.12}$$

where $\delta(\boldsymbol{x} - \boldsymbol{x}_0)$ is the Dirac delta distribution. In three-dimensional space Green's function is given as

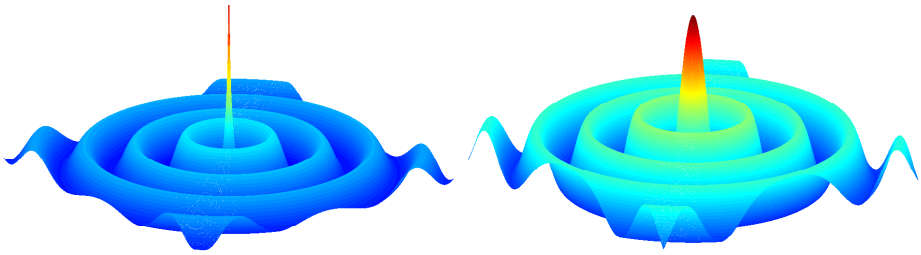
$$G(\boldsymbol{x}|\boldsymbol{x}_0) = \frac{e^{-\mathrm{i}k||\boldsymbol{x}-\boldsymbol{x}_0||}}{4\pi||\boldsymbol{x} - \boldsymbol{x}_0||}\,. \tag{2.13}$$

It is the solution to a point source in free-space at $\boldsymbol{x} = \boldsymbol{x}_0$. It is a spatio-temporal transfer function and as mentioned, a solution to any inhomogenuity can be found through the convolution with the Green's function [Wei12]. In Fig. 2.2 the real and imaginary part of Eq. 2.13 are plotted.

The Green's function fulfills the principle of acoustic reciprocity,

$$G(\boldsymbol{x}|\boldsymbol{x}_0) = G(\boldsymbol{x}_0|\boldsymbol{x})\,, \tag{2.14}$$

which states that the source and receiver are interchangeable with the receiver response staying the same [MF53] .



(a) real part (b) imaginery part

Figure 2.2: Green's function.

2.3.2 Helmholtz Integral Equation

The Helmholtz integral equation[3] (HIE) is the basis of many techniques in acoustics, e.g. wave field synthesis [SRA08], and represents the mathematical model of Huygen's principle [Jes73, GG06]. Assuming a time-harmonic sound field and no sources inside the domain of resolution V_i with a smooth boundary S (see Fig. 2.3) which is twice differentiable the HIE is given as

$$C(\boldsymbol{x})p(\boldsymbol{x}) = \iint_S \Big(G(\boldsymbol{x}|\boldsymbol{y}) \frac{\partial p(\boldsymbol{y})}{\partial \boldsymbol{n}} - p(\boldsymbol{y}) \frac{\partial G(\boldsymbol{x}|\boldsymbol{y})}{\partial \boldsymbol{n}} \Big) \mathrm{d}S(\boldsymbol{y}) \,, \tag{2.15}$$

where $G(\boldsymbol{x}|\boldsymbol{y})$ is a Green's function satisfying any kind of boundary condition with $\boldsymbol{x} \in \mathbb{R}^3$ and $\boldsymbol{y} \in S$, $\frac{\partial}{\partial \boldsymbol{n}}$ indicates the normal derivative, $\mathrm{d}S(\boldsymbol{y})$ means the integration wrt. the coordinate $\boldsymbol{y}$ and $C(\boldsymbol{x})$ is a constant defined as

$$C(\boldsymbol{x}) = \begin{cases} 0, & \boldsymbol{x} \in V_\mathrm{e} \,, \\ \frac{1}{2}, & \boldsymbol{x} \in S \,, \\ 1, & \boldsymbol{x} \in V_\mathrm{i} \,. \end{cases} \tag{2.16}$$

The HIE states that a continuous distribution of monopole and dipole sources on the surface of a closed domain weighted by the sound pressure and its normal derivative is sufficient to represent any kind of homogeneous and source-free sound field.

If the given problem requires specific boundary conditions, the Green's function satisfying these conditions has to be known. In case of a homo-

[3] In time domain this is usually called Kirchoff's integral equation. It is also often referred to as Kirchoff-Helmholtz integral (KHI).

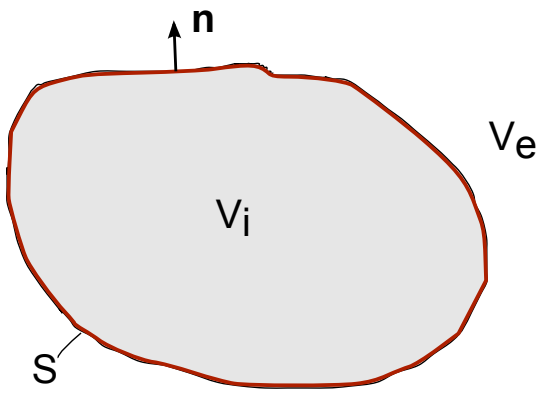


Figure 2.3: Region of definition for the HIE.

geneous Dirichlet boundary condition on the integration surface the HIE is reformulated as

$$C(\boldsymbol{x})p(\boldsymbol{x}) = -\iint_S p(\boldsymbol{y})\frac{\partial G_D(\boldsymbol{x}|\boldsymbol{y})}{\partial \boldsymbol{n}}\,\mathrm{d}S(\boldsymbol{y})\,, \tag{2.17}$$

where $G_D(\boldsymbol{x}|\boldsymbol{y})$ is the Dirichlet Green's function. In case of the homogeneous Neumann boundary condition the HIE becomes

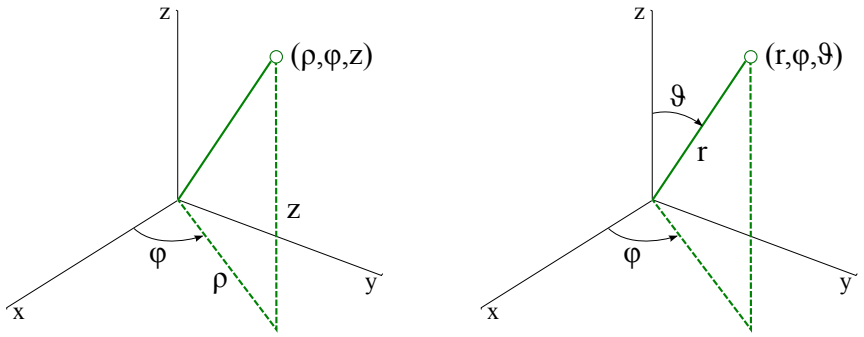
$$C(\boldsymbol{x})p(\boldsymbol{x}) = \iint_S G_N(\boldsymbol{x}|\boldsymbol{y})\frac{\partial p(\boldsymbol{y})}{\partial \boldsymbol{n}}\,\mathrm{d}S(\boldsymbol{y})\,, \tag{2.18}$$

where $G_N(\boldsymbol{x}|\boldsymbol{y})$ is the Neumann Green's function.

Green's functions, except for the free-field case, are usually not known and not trivial to derive for an arbitrarily shaped surface. Therefore, one can try to compute numerically from the HIE with free-field Green's function and its numerical implementation (cf. Ch. 3 and App. D) [Wil99].

2.4 Elementary Solutions of the Homogeneous Problem

This section sums up the solution of the homogeneous Helmholtz equation [MF53, Wil99, Zot09]. If a boundary value problem is given, it is evident to choose a coordinate system in which the boundary has a simple representation, e.g. a constant coordinate surface. The homogenous Helmholtz equation is solved by the separation of variables in the dedicated coordinate system. This always yields two types of harmonic solutions. If they fulfill the boundary conditions and the radiation condition as required, a superposition of these solutions leads to solutions of the inhomogeneous problem.



(a) Cylindrical (b) Spherical

Figure 2.4: Cylindrical and spherical coordinate system. Cylinder: $\rho = \sqrt{x^2+y^2}$, $\varphi = \arctan(\frac{y}{x})$ and $z = z$. Sphere: $r = \sqrt{x^2+y^2+z^2}$, $\varphi = \arctan(\frac{y}{x})$ and $\vartheta = \arccos\frac{z}{r}$. The domain of definitions are $r, \rho \in [0, \infty)$, $\varphi \in [0, 2\pi)$, $z \in (-\infty, \infty)$ and $\vartheta \in [0, \pi]$.

Here, the solutions in two orthogonal coordinate systems, the cylindrical and the spherical coordinates are presented (Fig. 2.4).

2.4.1 Cylindrical Coordinates

The separation of variables in cylindrical coordinates is given by

$$p(\boldsymbol{r}) = R(k\rho)\Phi(\varphi)Z(z) \; . \tag{2.19}$$

which yields three ordinary differential equations:

$$\begin{cases} \dfrac{\partial^2 R(k\rho)}{\partial\rho^2} + \dfrac{1}{\rho}\dfrac{\partial R(k\rho)}{\partial\rho} + (k_\rho^2 - \dfrac{n^2}{\rho^2})R(k\rho) = \; 0 \; , \\ \dfrac{\partial^2\Phi(\varphi)}{\partial\varphi^2} + m^2\Phi(\varphi) = \; 0 \; , \\ \dfrac{\partial^2 Z(z)}{\partial z^2} + k_z^2 Z(z) = \; 0 \; . \end{cases} \tag{2.20}$$

The numbers $m \in \mathbb{Z}$, $k_z \in (-\infty, \infty)$ and $k_\rho \in [0, \infty)$, are the separation constants used for the product ansatz, where k_ρ satisfies the dispersion relation $k_\rho = \sqrt{k^2 - k_z^2}$. Particularly, these equations are two second-order linear differential equations (in φ and z) and the Bessel equation (in $k\rho$).

Cylindrical Base-Solutions After solving these equations and choosing the solutions that are physical, the cylindrical base-solutions can be written as

$$p(k\rho,\varphi,z) = \sum_{n=-\infty}^{\infty} e^{in\varphi}\frac{1}{2\pi}\int_{-\infty}^{\infty}\Big[b_n J_n(k_\rho\rho) + c_n H_n^{(2)}(k_\rho\rho)\Big]e^{ik_z z}dk_z \quad (2.21)$$

where $n \in \mathbb{Z}$ and $k_z \in \mathbb{R}$, the coefficients b_n and c_n are the wave spectra of the interior and exterior wave field [Wil99], J_n are the Bessel functions and $H_n^{(2)}$ are the Hankel functions of second kind.

Eq. 2.21 is a complete synthesis operator, i.e., knowing the coefficients b_n and c_n of a certain problem means that homogeneous sound fields, valid in a given range of ρ, can be perfectly reconstructed. This is because the set of cylindrical basis functions are complete (cf. App. A). The corresponding analysis operator for the interior and exterior problem is given by ([GG06])

$$\begin{matrix} b_n \\ c_n \end{matrix} = \int_\rho\int_\varphi\int_z p(k\rho,\varphi,z) \begin{matrix} J_n(k_\rho\rho) \\ H_n^{(2)}(k_\rho\rho) \end{matrix} e^{i(n\phi+k_z z)}\,\rho\,\mathrm{d}\rho\,\mathrm{d}\varphi\,\mathrm{d}z\,. \quad (2.22)$$

Scattering off a Rigid Cylinder

The scattering of a plane wave incident on a rigid cylinder is most often described by assuming the cylinder to be of infinite length. The one dimensional plane waves scattered on an infinite cylinder only need to satisfy the radiation condition in the cylindrical radius. Hence the following solution is correct, cf. [Teu07, MI86, Wil99], for the sound pressure on the cylinder due to a plane wave from φ_0, ϑ_0

$$p(k,z,\varphi) = \sum_{m=-\infty}^{\infty} \frac{2\pi\,\mathrm{i}^{m+1}\,\Phi_m(\varphi_0)\,\Phi_m(\varphi)\,e^{\mathrm{i}k\cos\vartheta_0 z}}{k\,\mathrm{R}\,\sin\vartheta_0 H_m'^{(2)}(k\,\mathrm{R}\,\sin\vartheta_0)}, \quad (2.23)$$

where R is the radius of the cylinder, $H_n'^{(2)}(k\mathrm{R}\sin\vartheta_0)$ is the first derivative of the Hankel function of the second kind, and $\Phi_m(\varphi)$ are the normalized trigonometric functions

$$\Phi_m = \sqrt{\frac{2-\delta_m}{2\pi}}\begin{cases}\cos(m\varphi), & \text{for } m \le 0,\\ \sin(m\varphi), & \text{for } m < 0.\end{cases} \quad (2.24)$$

The term $k\,\mathrm{R}\,\sin\vartheta_0 H_n'^{(2)}(k\,\mathrm{R}\,\sin\vartheta_0)$ will not become zero for $\vartheta_0 = 0$; it is proportional to $\left(\frac{2}{k\,\mathrm{R}\,\sin\vartheta_0}\right)^n$ for small arguments.

The solution for a finite-length cylinder cannot be given in closed form [Teu07, p. 31], and fulfilling of the 3D radiation condition becomes necessary. It seems the scattering off a finite-length cylinder has to be simulated numerically.

2.4.2 Spherical Coordinates

Applying the separation of variables in spherical coordinates,

$$p(\boldsymbol{r}) = R(kr)\Phi(\varphi)\Theta(\vartheta) \tag{2.25}$$

it yields three ordinary differential equations:

$$\begin{cases} \dfrac{1}{r^2}\dfrac{\partial}{\partial r}\Big(r^2\dfrac{\partial R(kr)}{\partial r}\Big) + k^2 r - \dfrac{n(n+1)}{r^2}R(kr) = 0\,, \\ \dfrac{\partial^2\Phi(\varphi)}{\partial\varphi^2} + m^2\Phi(\varphi) = 0\,, \\ \dfrac{1}{\sin\vartheta}\dfrac{\partial}{\partial\vartheta}\Big(\sin\vartheta\dfrac{\partial\Theta(\vartheta)}{\partial\vartheta}\Big) + [n(n+1) - \dfrac{m^2}{\sin^2\vartheta}]\Theta(\vartheta) = 0\,. \end{cases} \tag{2.26}$$

The numbers $n \in \mathbb{Z}$ and $m \in \mathbb{Z}$ are the separation constants used for the product ansatz. Particularly, these equations are the spherical Bessel's equation, a standard second-order linear differential equation and an associated Legendre equation.

Spherical Base-Solutions After solving these equations and choosing the solutions that are physical [Zot09] the spherical base-solutions can be written as

$$p(kr, \boldsymbol{\theta}) = \sum_{n=0}^{\infty}\sum_{m=-n}^{n}\Big(b_{nm}\, j_n(kr) + c_{nm}\, h_n^{(2)}(kr)\Big)\, Y_n^m(\boldsymbol{\theta})\,, \tag{2.27}$$

where the unit vector $\boldsymbol{\theta} = (\varphi, \vartheta)^T$, the indices $n, m \in \mathbb{Z}$ are called the "order" and the "degree" of the expansion, the coefficients b_{nm} and c_{nm} are also called the wave spectra of the interior and exterior wave fields [Wil99], $j_n(kr)$ are the spherical Bessel functions, $h_n^{(2)}$ are the spherical Hankel functions of second kind and $Y_n^m(\boldsymbol{\theta})$ are the normalized real-valued spherical harmonics.. For a definition of these special functions see App. B.

Eq. 2.27 is a complete synthesis operator, i.e., knowing the coefficients b_{nm} and c_{nm} of a certain problem means the sound field bounded by one or two radii, can be perfectly reconstructed. The corresponding analysis operator for the interior and exterior problem is given by (cf. [GG06])

$$\begin{matrix} b_{nm} \\ c_{nm} \end{matrix} = \int_r \int_{\boldsymbol{\theta}} p(kr, \boldsymbol{\theta}) \begin{matrix} j_n(kr)\, Y_n^m(kr, \boldsymbol{\theta}) \\ h_n^{(2)}(kr)\, Y_n^m(kr, \boldsymbol{\theta}) \end{matrix} r^2 \mathrm{d}r\mathrm{d}\boldsymbol{\theta}\,. \tag{2.28}$$

Scattering off a Rigid Sphere

Assuming an incoming plane wave field impinging from the direction $\boldsymbol{\theta}_0$, the scattering response on the surface of a rigid sphere is given by

$$p(k, \boldsymbol{\theta}) = \sum_{n=0}^{\infty} \sum_{m=-n}^{n} \frac{4\pi \mathrm{i}^{n-1}\, Y_n^m(\boldsymbol{\theta}_0) Y_n^m(\boldsymbol{\theta})}{(k\,\mathrm{R})^2\, h_n'^{(2)}(k\mathrm{R})}\,, \tag{2.29}$$

where $h_n'^{(2)}(k\mathrm{R})$ is the derivative of the Hankel function of second kind and R is the radius of the sphere [Teu07].

2.5 Summary

This chapter reviewed some basics of analytical acoustics which are essential to this work. Especially the HIE will be used to represent scattering problems having homogeneous Neumann boundary conditions, similar to those results shown using homogeneous solutions. For the actual computation, a numerical implementation of the HIE has to be used. This is shown in the next chapter.

Chapter 3

Boundary Element Method

The boundary element method (BEM) is a numerical method to simulate homogeneous sound fields based on the knowledge of its boundary values or conditions on a discretized, arbitrarily shaped enclosing surface, so called boundary elements. It is based on the formulation of the physical problem as (boundary-) integral equations which is why the method was often referred to as boundary integral equation method[1] in its origins in the 1960's [Sch68, BM71]. The common formulation of the BEM in acoustics is based on the Helmholtz integral equation (HIE, cf. sec. 2.3.2).

The HIE is treated by approximation as a sum of integrals over boundary elements. The sound pressure has to be collocated to these elements using interpolating functions (shape functions) and the remaining integrals for each element are solved by numerical integration. The result is a linear system of equations characterized by two complex and fully occupied matrices. Further, the matrices are usually unsymmetric because of the non-uniform ares of the elements of a mesh [PKM12]. The solution of the matrix equation is costly.

An advantage of BEM is that the Sommerfeld radiation condition is inherently fulfilled. However, the reduction of dimensionality of the BEM also results in difficulties of non-uniqueness which do not exist in the original problem [BM71].

3.1 Basics

The basis of the BEM is the HIE, which is derived from the divergence theorem using Green's identities [CB91]. For the reader's connivance the

[1] This can still be the case when the derivation and analysis of the method is addressed rather than the implementation or application.

HIE for interior and exterior problems is rewritten here. The *Helmholtz integral equation for interior problems* is

$$C(\boldsymbol{x})p(\boldsymbol{x}) = \iint_S \Big(i\rho_o ck\, v_\mathrm{n}(\boldsymbol{x})G(\boldsymbol{x}|\boldsymbol{y}) - p(\boldsymbol{x})\frac{\partial G(\boldsymbol{x}|\boldsymbol{y})}{\partial \boldsymbol{n}}\Big)\mathrm{d}S(\boldsymbol{y}) + p^{(inc)}\ , \quad (3.1)$$

and the *Helmholtz integral equation for exterior problems* is

$$C(\boldsymbol{x})p(\boldsymbol{x}) = \iint_S \Big(p(\boldsymbol{x})\frac{\partial G(\boldsymbol{x}|\boldsymbol{y})}{\partial \boldsymbol{n}} - i\rho_o ck\, v_\mathrm{n}(\boldsymbol{x})G(\boldsymbol{x}|\boldsymbol{y})\Big)\mathrm{d}S(\boldsymbol{y}) + p^{(inc)}\,, \quad (3.2)$$

where $\boldsymbol{x} \in \mathbb{R}^3$ and $\boldsymbol{y} \in S$, $G(\boldsymbol{x}|\boldsymbol{y})$ is the free-field Green's function given in Eq. 2.13, $p(\boldsymbol{x})$ is the sound pressure, $p^{(inc)}$ is the sound pressure of an incoming field at the free-field boundary nodes (vanishes for a radiation problem), $\frac{\partial}{\partial \boldsymbol{n}}$ indicates the normal derivative and $C(\boldsymbol{x})$ is a constant defined depending on the problem. For the exterior problem it is

$$C(\boldsymbol{x}) = \begin{cases} 1, & \boldsymbol{x} \in V_\mathrm{e}\,, \\ \frac{\Omega(\boldsymbol{x})}{4\pi}, & \boldsymbol{x} \in S\,, \\ 0, & \boldsymbol{x} \in V_\mathrm{i}\,. \end{cases} \quad (3.3)$$

where $\Omega(\boldsymbol{x})$ is the solid angle defined by [Wei12]

$$\Omega(\boldsymbol{x}) \equiv \frac{1}{r^2}\iint_S \mathrm{d}S(\boldsymbol{x})\,. \quad (3.4)$$

where for smooth surfaces $\frac{\Omega(\boldsymbol{x})}{4\pi} = \frac{1}{2}$. The interior problem defines $C(\boldsymbol{x})$ just the other way around. In Fig. 2.3 the region of definition for the interior problem is shown.

3.1.1 Existence and Uniquness

There is one major shortcoming of the BEM. The HIE for exterior problems does not have a unique solution at certain frequencies. These characteristic eigenfrequencies are associated with the corresponding interior Dirichlet problem. If we consider an exterior problem with Dirichlet boundary condition the issue can be explained [WO02]. The HIE with $\boldsymbol{x} \in S$ becomes

$$\mathrm{i}\rho_o ck \int_S v_\mathrm{n}(\boldsymbol{x})\, G(\boldsymbol{x}|\boldsymbol{y})\, \mathrm{d}S(\boldsymbol{y}) = -\frac{1}{2}p(\boldsymbol{x}) - \int_S p(\boldsymbol{x})\, \frac{\partial G(\boldsymbol{x}|\boldsymbol{y})}{\partial \boldsymbol{n}}\, \mathrm{d}S(\boldsymbol{y})\,. \quad (3.5)$$

Further we have a look at the interior Dirichlet problem. With the surface normal unchanged the interior HIE becomes

$$\mathrm{i}\rho_o ck \int_S v_\mathrm{n}(\boldsymbol{x})\, G(\boldsymbol{x}|\boldsymbol{y})\, \mathrm{d}S(\boldsymbol{y}) = \frac{1}{2}p(\boldsymbol{x}) - \int_S p(\boldsymbol{x})\, \frac{\partial G(\boldsymbol{x}|\boldsymbol{y})}{\partial \boldsymbol{n}}\, \mathrm{d}S(\boldsymbol{y})\,. \qquad (3.6)$$

As the latter equation applies to interior problems it exhibits eigenfrequencies. The exterior problem does not have any eigenfrequencies but it shares the same term on the left-hand side. Hence, the non-uniqueness of the interior problem at certain frequencies also occurs in the HIE of the exterior problem. This issue arises purely from the mathematical approach and doesn't have any physical meaning. It is circumvented by additional strategies.

CHIEF

One simple method to overcome the non-uniqueness problem is the combined Helmholtz integral equation formulation (CHIEF) suggested by Schenk in 1968 [Sch68]. The idea is to add the HIE for interior points to the HIE for exterior points in order to remove the non-uniqueness due to interior modes. The interior HIE for exterior problems is

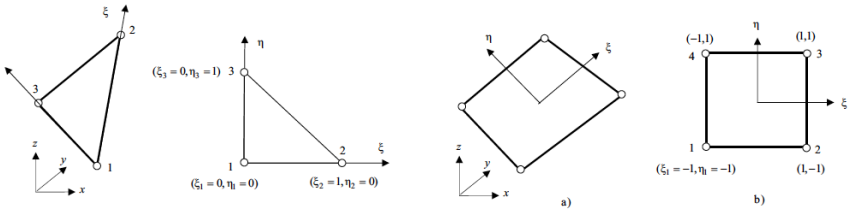
$$\iint_S \Big(p(\boldsymbol{x})\frac{\partial G(\boldsymbol{x}|\boldsymbol{y})}{\partial \boldsymbol{n}} - \mathrm{i}\rho_o ck\, v_\mathrm{n}(\boldsymbol{x}) G(\boldsymbol{x}|\boldsymbol{y})\Big)\mathrm{d}S(\boldsymbol{y}) = 0\,. \qquad (3.7)$$

This equation enforces a zero pressure condition inside the volume V and it can be seen as a constraint to the surface HIE. In general, the constraint equations for selected interior control points, the CHIEF points, are enough for the exterior problem to have a unique solution.

A challenge when using this method is the choice of suitably located CHIEF points. In particular if they are located at an interior nodal surface of an eigenfrequency the constraint becomes ineffective. This is especially problematic for higher frequencies where the nodal surfaces of the eigenfrequencies become more dense [Wu00, p. 27].

3.2 Numerical Implementation

The discretization of the HIE is done in two steps. First the boundary surface in consideration has to be discretized and second the boundary variables have to be discretized. In principal this can be done independently but in practice the geometry and the variables are mostly discretized in the same way which yields so called *isoparametric* elements. The shape of the elements in three-dimensions can either be of triangular or quadrilateral shape (Fig. 3.1).



(a) (b)

Figure 3.1: Real element (left) and parent element (right) a) Triangular b) Quadrilateral. From [Bee08].

The geometry is represented by nodes and so called shape functions which interpolate between the nodes. The number of nodes on an element determines the order of the shape functions. A constant element places one node at the centroid of the element. A linear element places nodes at the corners of the element. A quadratic element places nodes at the corners and in the middle of the edges. The integration is usually generalized and made on a parent or master element which means that every real element is transformed into local coordinates of the master element for integration. Part of the numerical error in the result is due to the approximation of the boundary. Therefore higher-order elements might be preferable. For a comprehensive treatment of elements and shape functions the reader is referred to standard BEM textbooks, e.g., [BW92] or a standard FEM book [ZT89].

Discretizing the boundary integral of the HIE leads to (the coordinate variables are left out for readability)

$$Cp = \sum_{j=1}^{\mathrm{M}} \int_{S_j} p \, \frac{\partial G}{\partial \mathrm{n}} \, dS - \mathrm{i}\rho_0 ck \sum_{j=1}^{\mathrm{M}} \int_{S_j} v_\mathrm{n} \, G \, dS \; . \tag{3.8}$$

where M is the number of elements. Next, the coordinates of the sound pressure are discretized using

$$p = \sum_{i=1}^{\mathrm{l}} p_i \, N_i(\xi_1, \xi_2), \tag{3.9}$$

where the index i indicates the nodal points, p_i is the collocated sound pressure, l is the number of nodes in that element and N_i are the shape functions defined on a master element in local coordinates ξ_1, ξ_2 [Wu00, p. 55]. This is called *collocation* or *nodal collocation*. Inserting Eq. 3.9 then yields

$$Cp = \sum_{j=1}^{\mathrm{M}} \sum_{i=1}^{\mathrm{l}} p_{ij}\, h_{ij} - \sum_{j=1}^{\mathrm{M}} \sum_{i=1}^{\mathrm{l}} v_{n,ij}\, g_{ij}\ . \tag{3.10}$$

where

$$h_{ij} = \int_{S_j} \frac{\partial G}{\partial n} N_i\, dS \tag{3.11}$$

are the dipole terms and

$$g_{ij} = \mathrm{i}\rho_0 ck \int_{S_j} G N_i\, dS \tag{3.12}$$

are the monopole terms. Finally, a matrix equation can be set up

$$\boldsymbol{Cp} = \boldsymbol{Hp} - \boldsymbol{Gv}_n\ , \tag{3.13}$$

where L the number of nodes, $\boldsymbol{C}$ is a $L \times M$ diagonal matrix containing the solid angles, $\boldsymbol{p}$ and $\boldsymbol{v}_{\mathrm{n}}$ are vectors of length L containing the sound pressure and the normal particle velocities at the nodes and $\boldsymbol{G}$ and $\boldsymbol{H}$ are $L \times M$ matrices given by

$$\boldsymbol{G} = \begin{pmatrix} g_{ij} & \cdots & g_{iM} \\ \vdots & \ddots & \vdots \\ g_{Lj} & \cdots & g_{LM} \end{pmatrix}, \boldsymbol{H} = \begin{pmatrix} h_{ij} & \cdots & h_{iM} \\ \vdots & \ddots & \vdots \\ h_{Lj} & \cdots & h_{LM} \end{pmatrix}.$$

For the solution of Eq. 3.13, first, the surface variables are solved for ($\boldsymbol{x} \in S$) where either the particle velocity or the sound pressure on the boundary is known. Then the computed vectors are inserted again into Eq. 3.13. This time it is solved for the sound pressure in the field ($\boldsymbol{x} \in V_{\mathrm{i}}$ or $\boldsymbol{x} \in V_{\mathrm{e}}$). In general a matrix equation of form

$$\boldsymbol{Ax} = \boldsymbol{b}\ , \tag{3.14}$$

has to be solved where matrix $\boldsymbol{A}$ and vector $\boldsymbol{b}$ contains the knowns and the vector $\boldsymbol{x}$ contains the unknowns.

3.3 Axisymmetric Formulation

A simplification of the HIE formulation for the BEM can be applied when a boundary is rotationally symmetric around the z-axis, as suggested by Juhl [Juh93] (axisymmetric formulation). In this case the HIE can be represented by an azimuthally harmonic Fourier series

$$p = \sum_{m=0}^{\infty} p_m \cos(m\varphi), \qquad v = \sum_{m=0}^{\infty} v_m \cos(m\varphi) \tag{3.15}$$

where m is the order of the expansion and φ is the angle in cylindrical coordinates. The discretization of the HIE is then carried out using Eq. 3.15. The advantage is that only a 2D contour of a 3D body has to be discretized. A full 3D solution is then achieved by assembling the solutions for single m. The Fourier expansion needs to be truncated and is therefore an approximation. However, depending on the problem a small number of expansion term can be sufficient. If a full axisymmetric description is required, the expansion with $m = 0$ is sufficient [CH01].

3.4 Summary

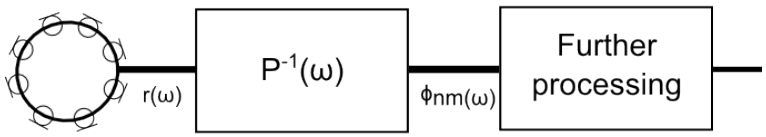
The BEM is the numerical implementation of the HIE and it therefore allows the computation of acoustic problems of arbitrary geometry. The accuracy of the results is depdendent on the density and the form of the mesh and on the frequency of interest. A very high mesh density is necessary for computations at high kr ($\lambda/6$ rule, cf. [Mar02]) and therefore the memory and computational load becomes high [CW07]. The Axisymmetric formulation reduces this problem and will be used in this thesis.

Chapter 4

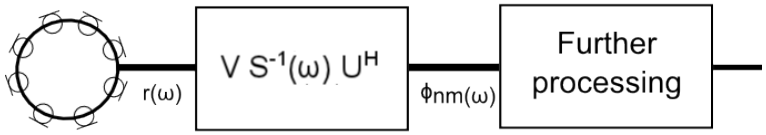
Modal Analysis of Free-Field Scatterers

Methods to find an acoustic modal representation of possible vibration patterns of the surface of arbitrary geometries were introduced since the beginning of the 1990's. Borgiotti [Bor90] suggested the use of the singular value decomposition (SVD) applied to a radiation operator representing the radiated power. Investigations on this concept for different applications can be found in [Pho90, Sar91, CC94]. Cunefare and Currey [CNC01] identified that the surface modes exhibit a grouping behavior concerning their modal strength and that the ones for a spherical geometry correspond to the spherical harmonics. These functions were named *acoustic radiation modes* (ARM) and the corresponding *radiation efficiency*. Nelson and Kahana [NK01] also used the SVD but applied it to a matrix of transfer functions (Green function matrix) acting in between a radiator and points in the far-field. The resulting functions corresponding to the ARM from before were named "source modes" and "field modes". Pasqual et al. [PdFAH10, PM11] applied the SVD analysis to obtain modal functions for the directivity control of loudspeaker arrays. They noted that insted of using spherical harmonics using ARMs has the advantage of optimally using all available degrees of freedom of the controlled surface is discretized.

In this work a slightly different approach is used. As we are interested in the modal representation of microphone arrays the SVD will be applied to the response of the microphone array to an impinging sound field. The scattering response on the boundary surface is computed employing the boundary element method (BEM, cf. Ch. 3) and the SVD is applied directly to the synthesized sound pressure. A spherical point-source distribution in the far-field is assumed to generated the incoming sound field. The results of this approach are similar to those of the cited works from above, but as the defini-



(a)



(b)

Figure 4.1: Block diagram of the signal processing steps for obtaining the acoustic model parameters. (a) shows the generic case where a matrix of transfer functions has to be inverted for each frequency. Fig. (b) shows the simplification using frequency independent array modes.

tions are different, the presented approach is not fully equivalent. Therefore, the terms array modes and modal strength will be used in contrast to acoustic radiation modes and radiation efficiencies, respectively.

The goal of this analysis is to find frequency and real-valued modal array modes. Fig. 4.1 shows a block-diagram of the signal processing necessary for beamforming or sound field reconstruction. Using frequency independent functions reduces the computational effort of the filtering steps considerably.

4.1 The Scattering Operator

In general, the scattered response of a rigid body $p^{(tot)}$ can be described as a superposition of an incoming sound field $p^{(inc)}$ and a scattered sound field $p^{(scat)}$

$$p^{(tot)} = p^{(inc)} + p^{(scat)} \,. \tag{4.1}$$

The scattered sound field can be thought of as a radiating sound field (due to acoustic reciprocity) that forces the normal particle velocity of the total field $p^{(tot)}$ on the boundary surface to zero.

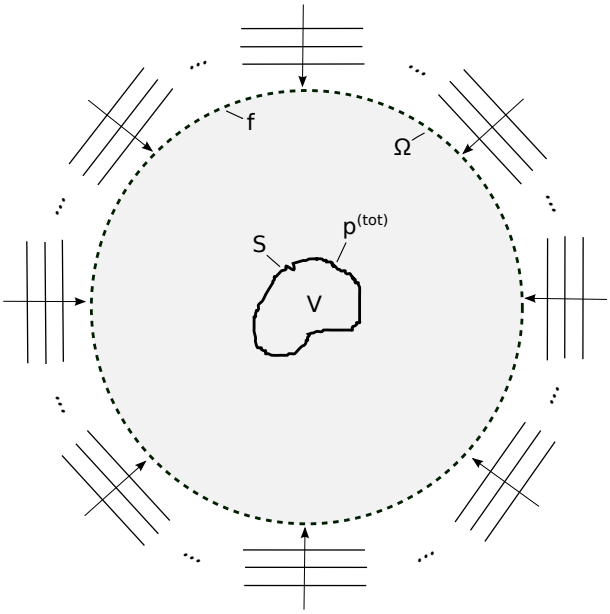


Figure 4.2: Region of definitions for the scattering problem with a continuous distribution of plane waves.

The scattering problem can be defined using integral operators [Faz10] in a similar manner to the HIE, presented in section 2.3.2. A sketch of the scattering problem is shown in Fig. 4.2. The sound pressure on the boundary surface S due to a spherical source distribution on Ω can be written as

$$p^{(tot)}(\boldsymbol{x}) = \int_{\Omega} f(\boldsymbol{y})\, P(\boldsymbol{x}|\boldsymbol{y})\, \mathrm{d}\Omega(\boldsymbol{y})\,. \tag{4.2}$$

where $f(\boldsymbol{x})$ is the source strenght or density function and $P(\boldsymbol{x}|\boldsymbol{y})$ is a wave satisfying

$$\begin{cases} (\Delta + k^2)P(\boldsymbol{x}|\boldsymbol{y}) = & -\delta(\boldsymbol{x}-\boldsymbol{y}),\, \boldsymbol{x} \in \mathbb{R}^3 \backslash V, \boldsymbol{y} \in \Omega \\ \dfrac{\partial P(\boldsymbol{x}|\boldsymbol{y})}{\partial \mathbf{n}} = & 0\,,\, \boldsymbol{x} \in S\,, \end{cases} \tag{4.3}$$

where S is the surface of the scattering body V. This equation demands that P satisfies the homogeneous Helmholtz equation in all space except the region V and additionally satisfies the Neumann boundary condition on the scattering surface S. P represents a general wave field, but in fact a Green's function or a Herglotz wave function (plane wave) satisfying the same conditions could be used. In order to write down Eq. 4.2 in a more

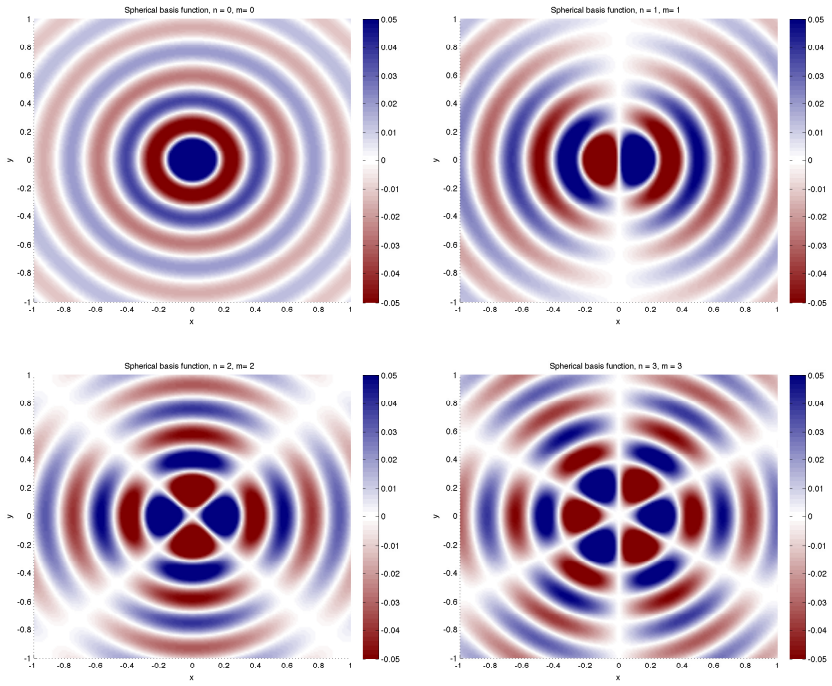


Figure 4.3: Spherical basis functions for n=0-3 and m=n.

compact way, operator notation is used,

$$p^{(tot)}(\boldsymbol{x}) = (\mathcal{P}\, f)(\boldsymbol{x})\,, \tag{4.4}$$

where the operator $\mathcal{P}$ is defined as acting from the source distribution Ω to the rigid boundary S ($\mathcal{P} : \Omega \to S$) and represents the integral operation from the right-hand side of Eq. 4.2.

When a reconstruction of these parameters is demanded the operator $\mathcal{P}$ has to be inverted. This is the problem beamforming and source reconstruction techniques try to solve [Wil99, VW04, Faz10].

4.1.1 Spherical Source Distribution

The incoming sound field is generated assuming a spherical distribution of point sources at the radius $\mathrm{r_s}$. The Helmholtz equation excited by this source distribution is written as

$$(\Delta + k^2)p^{(inc)}(r, \boldsymbol{\theta}) = -\frac{\delta(r - \mathrm{r_s})}{{\mathrm{r_s}}^2}\, f(\boldsymbol{\theta})\,, \tag{4.5}$$

where Δ is the Laplace operator, k the wavenumber, δ a Dirac delta distribution, $p^{(inc)}$ is the sound pressure with $(r, \boldsymbol{\theta}) \in \mathbb{R}^3$ and $f(\boldsymbol{\theta})$ is a continuous source strength equivalent to the one form the previous section. The solution of this problem for $r < \mathrm{r_s}$ can be given as (cf. [ZPF09])

$$p^{(inc)}(kr, \boldsymbol{\theta}) = -\mathrm{i}k \sum_{n=0}^{\infty} h_n^{(2)}(k\mathrm{r_s})\, j_n(kr) \sum_{m=-n}^{n} \phi_{nm}\, Y_n^m(\boldsymbol{\theta})\,, \tag{4.6}$$

where j_n are the spherical Bessel functions, $h_n^{(2)}$ the spherical Hankel functions of second kind, Y_n^m are the real-valued spherical harmonics (cf. App. B.3) and

$$\begin{aligned} f(\boldsymbol{\theta}) &= \sum_{n=0}^{\infty} \sum_{m=-n}^{n} \phi_{nm} Y_n^m(\boldsymbol{\theta})\,, \\ \phi_{nm} &= \int_{\Omega} f(\boldsymbol{\theta}) Y_n^m(\boldsymbol{\theta})\, \mathrm{d}\Omega\,, \end{aligned} \tag{4.7}$$

are the coefficients of the expansion. Moreover, assuming the source distribution to be in the far-field ($\mathrm{r_s} >> r$), using the far-field approximation of the spherical Hankel functions ($h_n^{(2)}(kr) = \frac{\mathrm{i}^{n+1} e^{-\mathrm{i}kr}}{kr}$) and equalizing by $\frac{4\pi r}{e^{-\mathrm{i}kr}}$ results in a continuous distribution of plane waves given by

$$p^{(inc)}(kr, \boldsymbol{\theta}) = 4\pi \sum_{n=0}^{\infty} \mathrm{i}^n\, j_n(kr) \sum_{m=-n}^{n} \phi_{nm}\, Y_n^m(\boldsymbol{\theta})\,. \tag{4.8}$$

Now, we let $\phi_{nm} = \delta_{nn'}\delta_{mm'}$, where δ indicates the Kronecker delta and $nm = n^2 + n + m + 1$ is the running index of the spherical harmonics. This creates a superposition of plane waves expressed by spherical wave functions where on wave is given by

$$p_{nm}^{(inc)}(kr, \boldsymbol{\theta}) = 4\pi \mathrm{i}^n\, j_n(kr)\, Y_n^m(\boldsymbol{\theta})\,. \tag{4.9}$$

In [GD04] these waves were called spherical basis functions and Fig. 4.3 shows some of them. Fig. 4.2 depicts a model of the incoming sound field.

Using this kind of representation of the incoming sound field the scattering operator can be rewritten to

$$p^{(tot)}(\boldsymbol{x}) = \Big(\mathcal{P}_{nm}\, \phi_{nm}\Big)(\boldsymbol{y})\,, \tag{4.10}$$

where $p^{(tot)}(\boldsymbol{x})$ is the total sound pressure and $\mathcal{P}_{nm}$ is the spherical basis function expanded operator $\mathcal{P}$. The expansion coefficients ϕ_{nm} define the sound field of the source and hence they represent the parameters of the acoustic model.

4.2 Scattering Matrix via BEM

The scattered sound field for arbitrary geometries can be written in terms of the Helmholtz integral equation (HIE) presented in section 2.3.2. Applying a boundary condition for a rigid surface, $\frac{\partial p(\boldsymbol{y})}{\partial \mathbf{n}} = 0$, the total sound pressure is

$$\alpha\, p^{(tot)}(\boldsymbol{x}) = \int_S p^{(tot)}(\boldsymbol{y})\, \frac{\partial G(\boldsymbol{x}|\boldsymbol{y})}{\partial \boldsymbol{n}} \mathrm{d}S(\boldsymbol{y}) + p^{(inc)}\,, \tag{4.11}$$

where $\boldsymbol{y} \in S$, $\boldsymbol{x} \in \mathbb{R}^3 \backslash V$ and α is the solid angle and for smooth surface $\alpha = \frac{1}{2}$. Discretizing the boundary using L elements and nodes (standard collocation) results in a matrix equation

$$\boldsymbol{C}\boldsymbol{p}^{(tot)} = \boldsymbol{H}\boldsymbol{p}^{(tot)} + \boldsymbol{p}^{(inc)}\,, \tag{4.12}$$

where $\boldsymbol{H} \in \mathbb{R}^{\mathrm{L}\times\mathrm{L}}$ is the matrix of the normal derivatives of the Green's functions integrated over a single element (cf. 3), $\boldsymbol{p}^{(tot)} \in \mathbb{R}^{\mathrm{L}\times 1}$ and $\boldsymbol{p}^{(inc)} \in \mathbb{R}^{\mathrm{L}\times 1}$ are the vectors of the unknown sound pressures and the sound pressure of the incoming field at the surface nodes in the open field, respectively, and $\boldsymbol{C} \in \mathbb{R}^{\mathrm{L}\times\mathrm{L}}$ is a diagonal matrix containing the solid angles.

Furthermore, using the incoming sound field defined in Eq. 4.8 in matrix form yields

$$\boldsymbol{p}^{(inc)} = \boldsymbol{R}\boldsymbol{\phi}\,, \tag{4.13}$$

where $\boldsymbol{\phi} \in \mathbb{R}^{(\mathrm{N}+1)^2\times 1}$ are the spherical harmonics coefficients and $\boldsymbol{R} \in \mathbb{R}^{\mathrm{L}\times(\mathrm{N}+1)^2}$ is a matrix including the single spherical wave components from Eq. 4.9

$$\boldsymbol{R} = \begin{pmatrix} j_0(kr_0)Y_0^0(\boldsymbol{\theta}_0) & \cdots & j_{\mathrm{N}}(kr_0)Y_{\mathrm{N}}^{\mathrm{N}}(\boldsymbol{\theta}_0) \\ \vdots & \ddots & \vdots \\ j_0(kr_{\mathrm{L}})Y_0^0(\boldsymbol{\theta}_{\mathrm{L}}) & \cdots & j_{\mathrm{N}}(kr_{\mathrm{L}})Y_{\mathrm{N}}^{\mathrm{N}}(\boldsymbol{\theta}_{\mathrm{L}}) \end{pmatrix}\,, \tag{4.14}$$

where N is the order of the spherical harmonics expansion and $(N+1)^2$ is the number of spherical waves for which $n \leq N$. The discrete total scattered sound pressure on the boundary surface S is then given by

$$\boldsymbol{p}^{(tot)} = \underbrace{-(\boldsymbol{H}-\boldsymbol{C})^{-1}\boldsymbol{R}}_{\boldsymbol{P}_{nm}}\boldsymbol{\phi}\,, \tag{4.15}$$

where $\boldsymbol{P}_{nm}$ is the scattering matrix and consists of the responses to the single spherical wave $\boldsymbol{p}_{nm}$. It is the discrete equivalent to the scattering operator Eq. 4.10 and given by

$$\boldsymbol{P}_{nm} = (\boldsymbol{p}_{00}, \ldots, \boldsymbol{p}_{nm}, \ldots, \boldsymbol{p}_{NN})\,. \tag{4.16}$$

Reconstruction of the sound field or beamforming demand the inversion of the scattering matrix (cf. C).

4.2.1 SVD of the Scattering Matrix

The SVD of the scattering matrix is given by

$$\boldsymbol{P} = \boldsymbol{U}\boldsymbol{\Sigma}\boldsymbol{V}^{\mathbf{H}}, \tag{4.17}$$

where $\boldsymbol{U} \in \mathbb{R}^{L\times L}$ contains the left singular vectors in its columns, $\boldsymbol{V} \in \mathbb{R}^{(N+1)^2\times(N+1)^2}$ contains the right singular vectors and $\boldsymbol{\Sigma} \in \mathbb{R}^{L\times(N+1)^2}$ is a diagonal matrix of the singular values in decreasing order

$$|\sigma_1| \geq |\sigma_2| \geq \ldots \geq |\sigma_N|. \tag{4.18}$$

The left and right singular vectors form a set of orthonormal vectors

$$\boldsymbol{U}^{\mathbf{H}}\boldsymbol{U} = \boldsymbol{I}\,, \quad \boldsymbol{V}^{\mathbf{H}}\boldsymbol{V} = \boldsymbol{I}\,, \tag{4.19}$$

where $\boldsymbol{I}$ is the identity matrix. The physical interpretation of the singular vectors and values in this context is not that easy. We can try to understand them when the SVD is related to the eigenvalue decomposition. Multiplying the scattering matrix from the right by its complex conjugate yields

$$\boldsymbol{P}\boldsymbol{P}^{\mathbf{H}} = \boldsymbol{U}\boldsymbol{\Sigma}\boldsymbol{\Sigma}^{\mathbf{H}}\boldsymbol{U}^{\mathbf{H}}\,. \tag{4.20}$$

In this case $\boldsymbol{P}\boldsymbol{P}^{\mathbf{H}} \in \mathbb{R}^{L\times L}$ represent the scalar product of the row vectors of $\boldsymbol{P}$ with the complex conjugated row vectors of $\boldsymbol{P}$. The corresponding eigenvectors $\boldsymbol{U}$ yield basis vectors which are only dependent on the geometry of S (the array) and the frequency. The can be seen as being equivalent to the ARMs mentioned in the introduction and will be called *array modes*.

Similarly, multiplying the scattering matrix by its complex conjugate yields

$$\boldsymbol{P}^{\mathbf{H}}\boldsymbol{P} = \boldsymbol{V}^{\mathbf{H}}\boldsymbol{\Sigma}^{\mathbf{H}}\boldsymbol{\Sigma}\boldsymbol{V}. \tag{4.21}$$

In this case $\boldsymbol{P}^{\mathbf{H}}\boldsymbol{P} \in \mathbb{R}^{(N+1)^2\times(N+1)^2}$ means the scalar product of the column vectors of $\boldsymbol{P}$ and the complex conjugated column vectors of $\boldsymbol{P}$. As the incoming sound field is defined by a set of orthogonal functions and if the scattering response does not shape these functions severely the matrix $\boldsymbol{V}$ yields the identity matrix. It will be shown that this is the case for low frequencies. However, as soon as the wavelength corresponds to the size of the scattering body this holds no longer.

In both cases the singular values $\boldsymbol{\Sigma}$ are the square-roots of the eigenvalues and they relate the impinging spherical wave components to the modes of the array.

4.2.2 Joint SVD

As claimed in the introduction, the goal is to find array modes that are real and independent of frequency and therefore a separation of the sound field into functions dependent on the surface variable and functions dependent on frequency and/or scaling can be achieved. The SVD, as described above, yields singular vectors only for one frequency. It has be shown that for certain array geometries these functions are frequency independent [PM11]. However, as soon as the singular values of the decomposition do not follow a clear degenerative pattern anymore, the singular vectors will be different for each frequency. Nevertheless, it may be possible that these matrices share the same diagonalization and we can try to find these vectors using a joint SVD or joint eigendecomposition [CS96]. The principle is as follows:

Given Z matrices $A_z \in \mathbb{R}^{\mathrm{j}\times\mathrm{j}}$

$$\{\boldsymbol{A}_1, \boldsymbol{A}_2, \ldots, \boldsymbol{A}_\mathrm{Z}\} \tag{4.22}$$

one can try to find a joint eigendecomposition so that

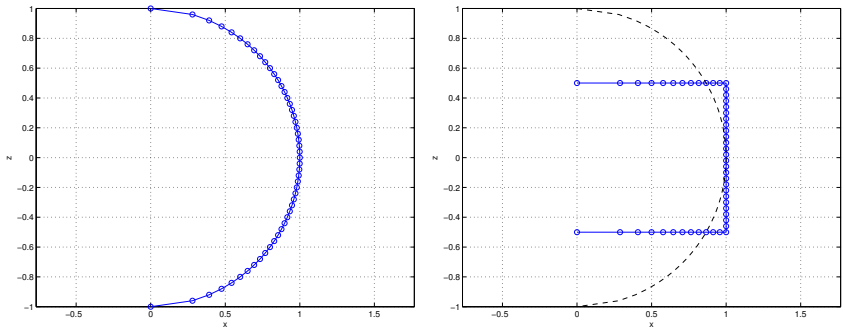
$$\{\boldsymbol{\Sigma}_1, \boldsymbol{\Sigma}_2, \ldots, \boldsymbol{\Sigma}_\mathrm{Z}\} = \{\boldsymbol{U}^\mathrm{H}\boldsymbol{A}_1\boldsymbol{V}, \boldsymbol{U}^\mathrm{H}\boldsymbol{A}_2\boldsymbol{V}, \ldots, \boldsymbol{U}^\mathrm{H}\boldsymbol{A}_\mathrm{Z}\boldsymbol{V}\} \tag{4.23}$$

where each $\boldsymbol{\Sigma}_k$ is as diagonal as possible. Further, if $A_z \in \mathbb{R}^{\mathrm{j}\times 1}$ then the joint SVD using a joint eigendecomposition can be defined as [Hor09]

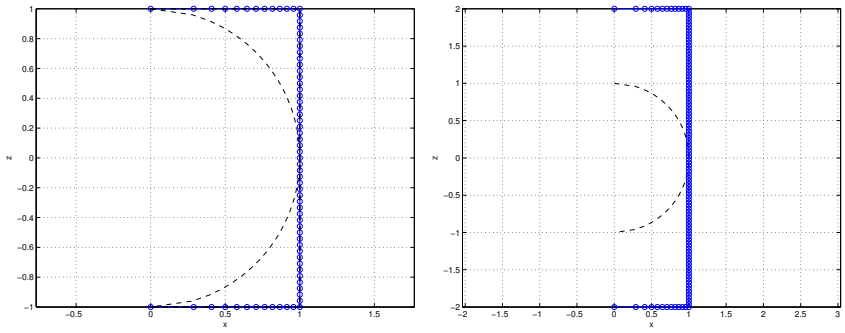
$$\{\boldsymbol{\Sigma}_1\boldsymbol{\Sigma}_1^\mathrm{H}, \boldsymbol{\Sigma}_2\boldsymbol{\Sigma}_2^\mathrm{H}, \ldots, \boldsymbol{\Sigma}_\mathrm{Z}\boldsymbol{\Sigma}_\mathrm{Z}^\mathrm{H}\} = \{\boldsymbol{U}\boldsymbol{A}_1\boldsymbol{A}_1^\mathrm{H}\boldsymbol{U}^\mathrm{H}, \boldsymbol{U}\boldsymbol{A}_2\boldsymbol{A}_2^\mathrm{H}\boldsymbol{U}^\mathrm{H}, \ldots, \boldsymbol{U}\boldsymbol{A}_\mathrm{Z}\boldsymbol{A}_\mathrm{Z}^\mathrm{H}\boldsymbol{U}^\mathrm{H}\}\,. \tag{4.24}$$

Of course an exact solution of this problem is only achievable if the matrices A_z actually share the same singular vectors. If otherwise, an approximation has to be used. An algorithm which tries to minimize the off-diagonal terms of $\boldsymbol{\Sigma}_z$ can be found in [CS96].

In the context of this work a joint SVD will be computed, of several scattering matrices $\boldsymbol{P}_{nm}$ for different frequencies, using the algorithm mentioned before.



(a) $R = 1$ (b) $\frac{R}{L} = \frac{1}{0.5}$



(c) $\frac{R}{L} = \frac{1}{1}$ (d) $\frac{R}{L} = \frac{1}{2}$

Figure 4.4: Generator meshes used for the BEM.

4.3 Simulation Results

Two examples are shown to evaluate the presented method. The first case is a rigid spherical array and as a second case rigid cylindrical arrays of different dimensions are simulated.

For the computation of the scattering matrix, the axisymmetric BEM formulation is used [Juh93]. This means that the problem is reduced to one dimension and modal functions can be found that dependent on one coordinate and the frequency only. Further, only the generator of the rigid body has to be discretized. For the BEM the open source Matlab toolbox *OpenBEM* is used which was written by Peter Juhl and Vicente Cutanda-Henriquez [CHJ10].

Fig. 4.4 shows the generators used for simulation. It has to be noted that the density of the nodal points on the generators is large which yields "quasi-continuous" singular functions. An example of practical relevance having less sampling points is not presented here. The incoming sound field is generated for single spherical waves up to fifth order and positive degree m only.

4.3.1 Sampling of the Generator

Nelson and Kahana [NK01] have already found that the results of the SVD are dependent on the choice of the mesh used for the BEM. Furthermore, Peters and Marburg [PKM12] remarked that the BEM matrices are not symmetric and therefore yield ARMs that are complex and unphysical in the context of radiated power.

Here, the sampling of the generator is chosen so that the generated surface areas are of equal area. It is evident that the choice of the axisymmetric BEM formulation yields a further advantage because a regular discretization is fairly easier to fulfill.

4.3.2 Sphere

The modal representation based on spherical waves of a plane wave scattered by a rigid sphere is given by (cf. [Zot09])

$$p^{(tot)}(kr,\boldsymbol{\theta}) = \sum_{n=0}^{\infty} 4\pi \mathrm{i}^n \left(j_n(kr) - \frac{j_n^{'}(kR)}{h_n^{(2)'}(kR)} h_n^{(2)}(kr) \right) \times \sum_{m=-n}^{n} Y_n^m(\boldsymbol{\theta}) Y_n^{m^*}(\boldsymbol{\theta}_0)\,, \tag{4.25}$$

where $\boldsymbol{\theta}_0$ represents the incidence direction, R is the radius of the sphere and the prime indicates the first derivative. Using the Wronski determinant $j_n(kR)h_n^{(2)'}(kR) - j_n^{'}(kr_y)h_n^{(2)}(kr_y) = \frac{1}{\mathrm{i}(kR)^2}$ it becomes

$$p^{(tot)}(kR,\boldsymbol{\theta}) = 4\pi \sum_{n=0}^{\infty} \frac{\mathrm{i}^{n-1}}{(kR)^2\, h_n^{(2)'}(kR)} \sum_{m=-n}^{n} Y_n^m(\boldsymbol{\theta}) Y_n^{m^*}(\boldsymbol{\theta}_0). \tag{4.26}$$

This directly indicates that the SVD will give singular vectors corresponding to the spherical harmonics and the singular values that correspond to the derivative and inverse of the Hankel functions (cf. [NK01]). The singular values must be real, however.

SVD for various frequencies

The SVD was conducted at different logarithmically spaced frequencies ($kr = 0.1 - 10$, using 12 values) and the dimensions are kept fixed throughout the simulations. The development of the singular values can be seen in Fig.

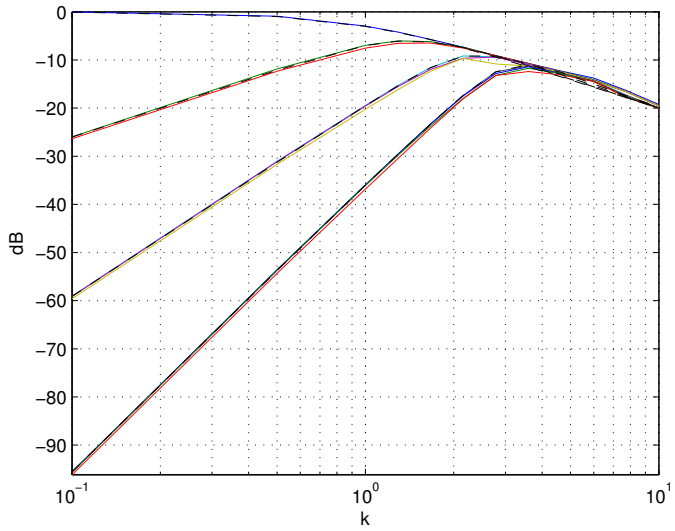


Figure 4.5: Sphere. The colored lines show the ten strongest singular values over frequency ($kr = 0.1 - 10$ in 12 logarithmically spaced steps). The black dashed line plots $\frac{1}{(kr)^2 h_n^{(2)}(kr)}$.

4.5. The clear frequency dependence and the correspondence to the inverse of the derivative of the spherical Hankel functions can be seen. Fig. 4.6 shows the singular vectore $\boldsymbol{U}$ corresponding to the strongest six singular values. The modes for $kr = \{0.1, 0.5, 1\}$ are plotted. It can be seen that the modes are nearly equal. Fig. 4.7 shows the singular vectors $\boldsymbol{V}$ for different frequencies. At low frequencies $\boldsymbol{V}$ is the identity matrix which means the scattering response of one spherical wave component is independent of all other responses. For frequencies $k > 1$ this does not hold anymore.

4.3.3 Cylinder

The modal analysis is applied to finite-length cylindrical arrays of different dimensions. The generator models are shown in Fig. 4.4, where R is the radius and 2L the height of the cylinder. The dimensions are kept fixed throughout the simulations.

SVD for various frequencies

Figs. 4.8 (a)-(c) show the singular values over frequency. Dependending on the dimensions the values differ compared to the sphere and also inside the groups the values change. Further, the singular values become more uniform

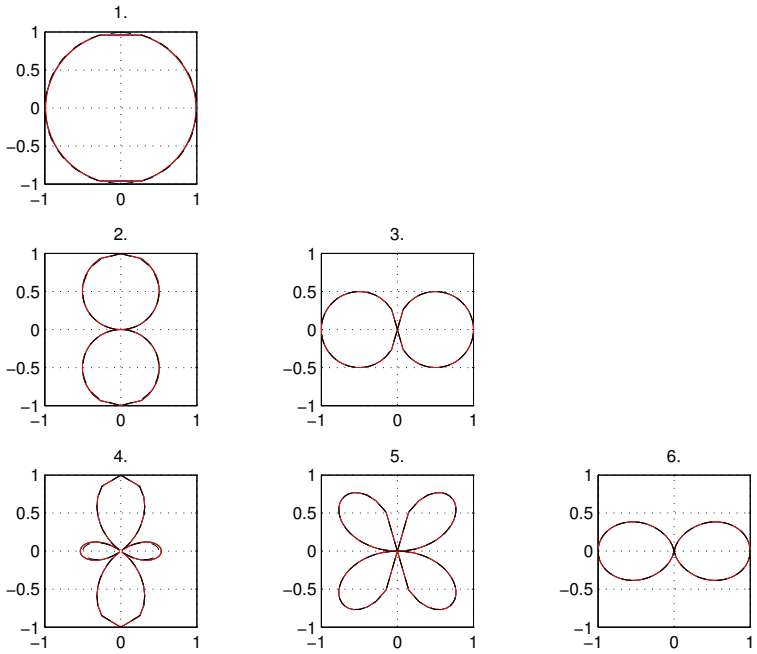


Figure 4.6: Sphere. Singular vectors $\boldsymbol{U}$ at $\{kR = 0.1, 0.5, 1\}$ colored and associated Legendre functions in black dashed.

up from $kr \approx 1$. Figs. 4.9 - 4.11 show the singular vectors $\boldsymbol{U}$ for low frequencies. It can be seen that the shape differs compared to the sphere but the zero-crossing and peaks of the modes remain the same. This indicates that the cylindrical array modes are distorted version of the spherical array modes. Figs. 4.12-4.14 show the singular vectors $\boldsymbol{V}$. Again, at low frequencies the identity matrix results and for higher frequencies the SVD starts to mix the modes and is not unique anymore.

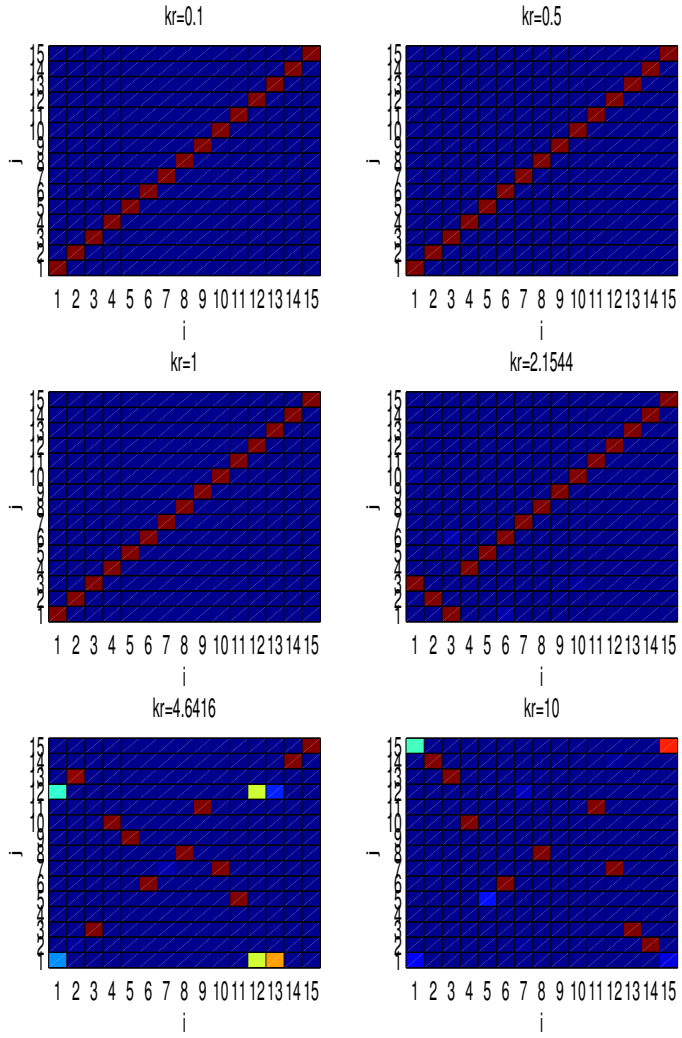
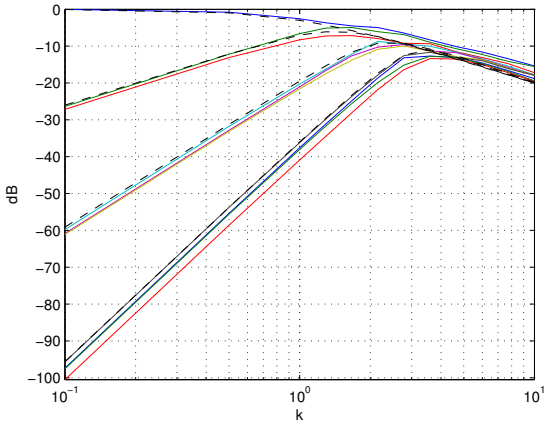
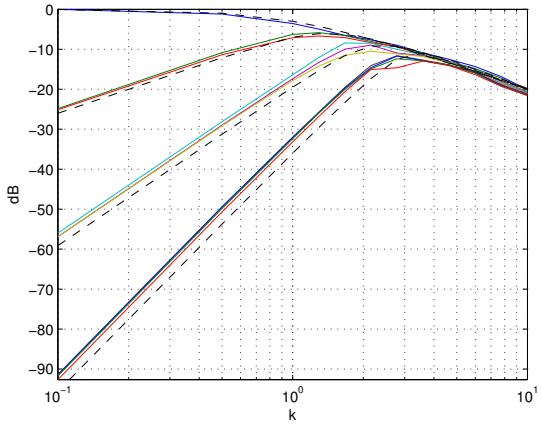


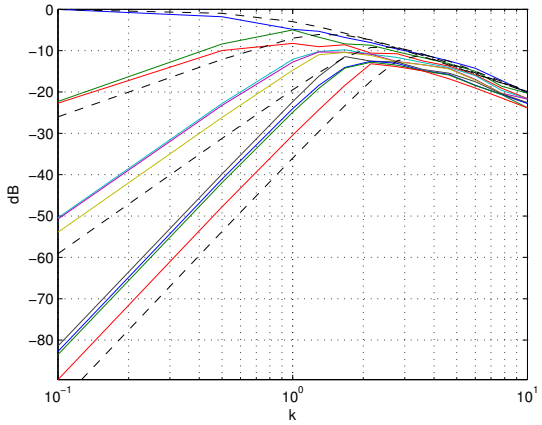
Figure 4.7: Sphere. Singular vectors $\boldsymbol{V}$ at several frequencies. The color indicates a scale from 0 (blue) to 1 (red) and the indices stand for the i-th column and j-th row of $\boldsymbol{V}$.



(a)



(b)



(c)

Figure 4.8: Cylinder (a) $\frac{R}{L} = \frac{1}{0.5}$, (b) $\frac{R}{L} = \frac{1}{1}$, (c) $\frac{R}{L} = \frac{1}{2}$. The colored lines show the ten strongest singular values over frequency (k=0.1-10 in 12 logarithmically spaced steps). The black dashed line plots $\frac{1}{(kr)^2 h_n^{(2)}(kr)}$.

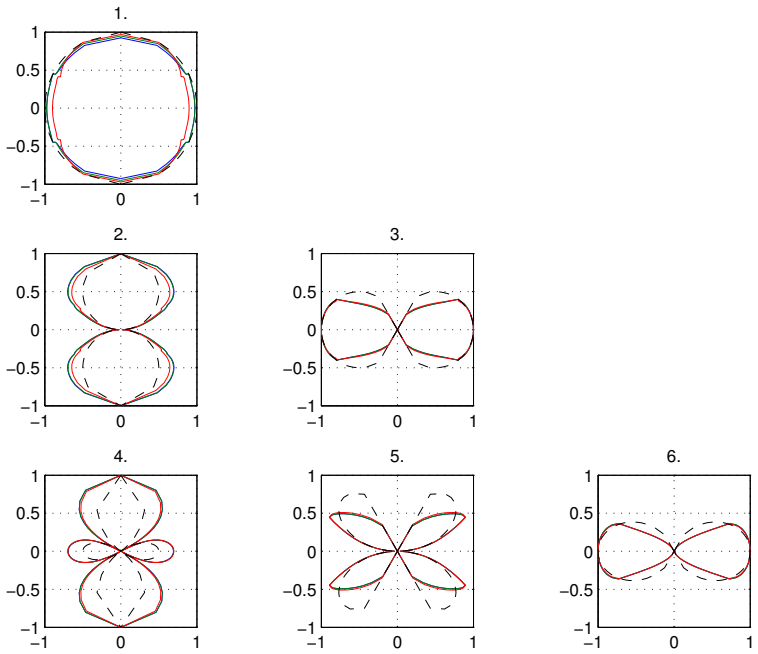


Figure 4.9: Cylinder $\frac{R}{L} = \frac{1}{0.5}$. Singular vectors $\boldsymbol{U}$ at $kR = \{0.1, 0.5, 1\}$ colored and associated Legendre functions in black dashed.

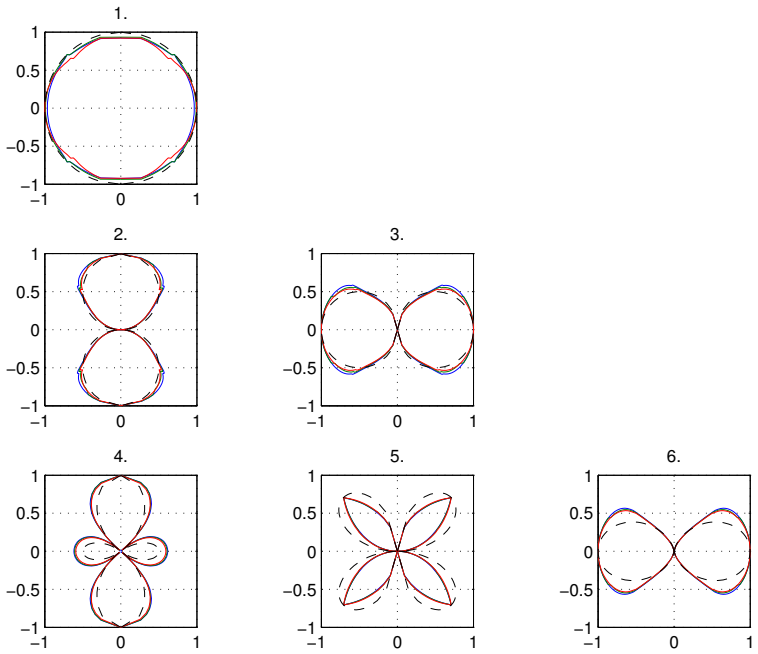


Figure 4.10: Cylinder $\frac{R}{L} = \frac{1}{1}$. Singular vectors $\boldsymbol{U}$ at $kR = \{0.1, 0.5, 1\}$ colored and associated Legendre functions in black dashed.

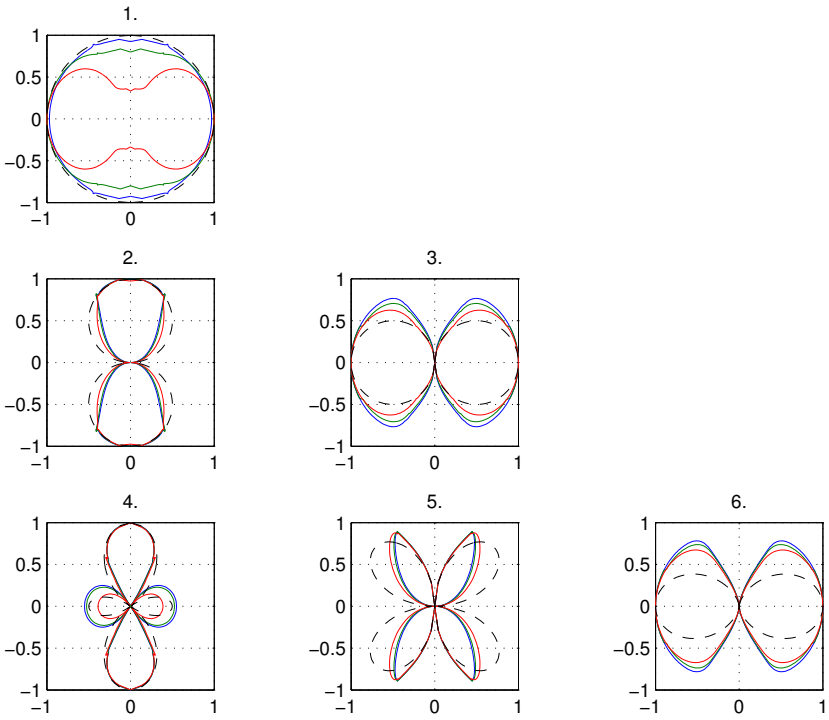


Figure 4.11: Cylinder $\frac{R}{L} = \frac{1}{2}$. Singular vectors $\boldsymbol{U}$ at $kR = \{0.1, 0.5, 1\}$ colored and associated Legendre functions in black dashed.

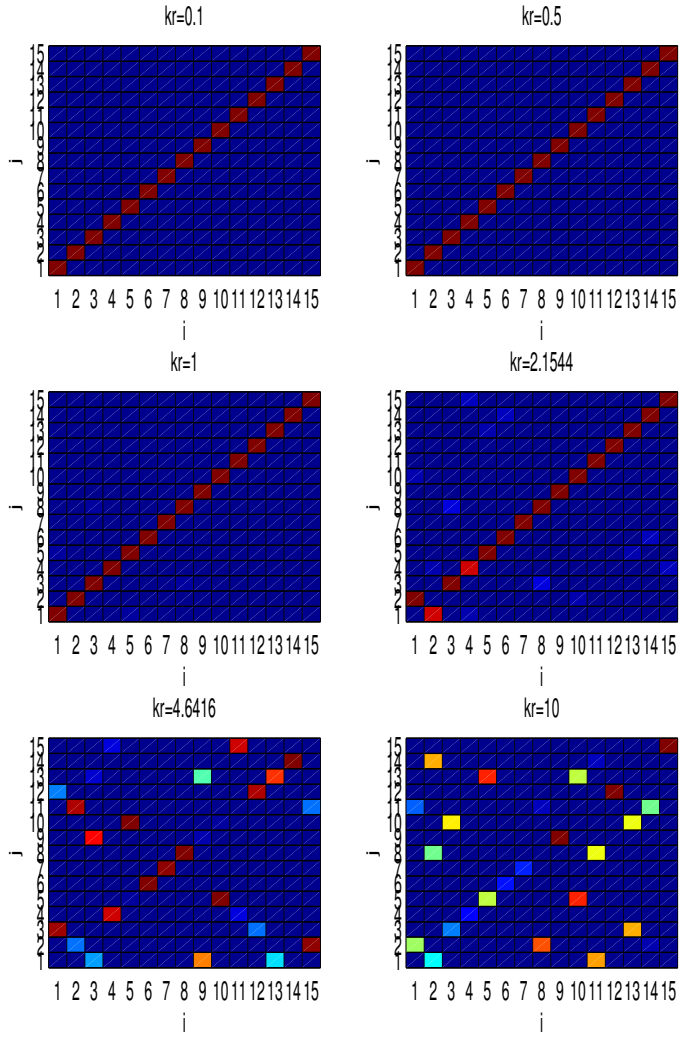


Figure 4.12: Cylinder $\frac{R}{L} = \frac{1}{0.5}$. Singular vectors $\boldsymbol{V}$ at several frequencies. The color indicates a scale from 0 (blue) to 1 (red) and the indices stand for the i-th column and j-th row of $\boldsymbol{V}$.

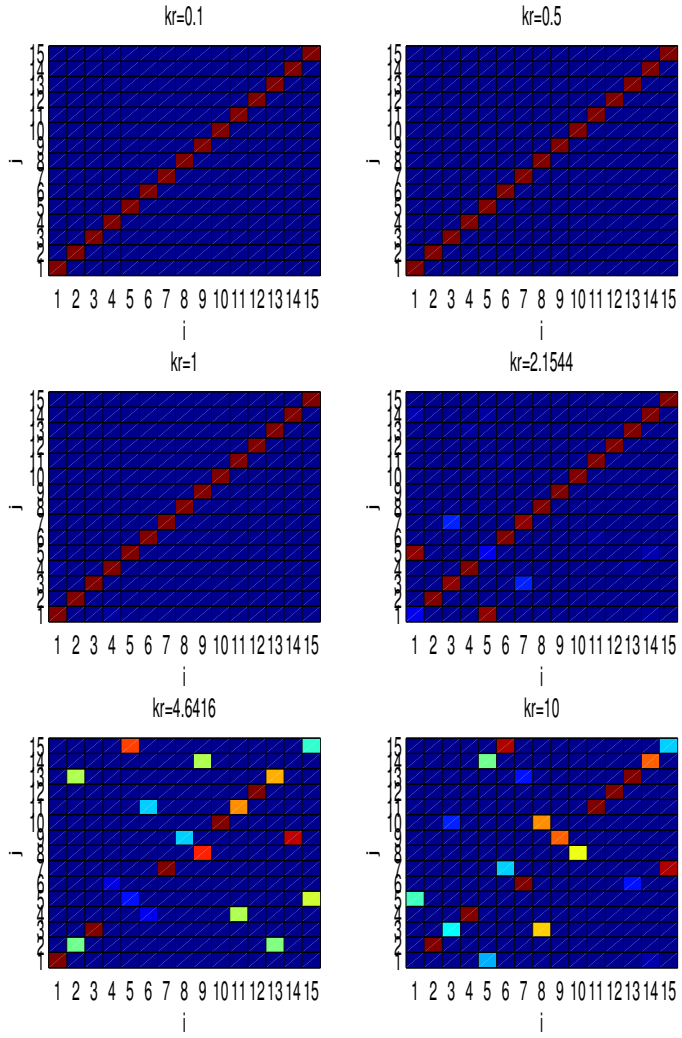


Figure 4.13: Cylinder $\frac{R}{L} = \frac{1}{1}$. Singular vectors $\boldsymbol{V}$ at several frequencies. The color indicates a scale from 0 (blue) to 1 (red) and the indices stand for the i-th column and j-th row of $\boldsymbol{V}$.

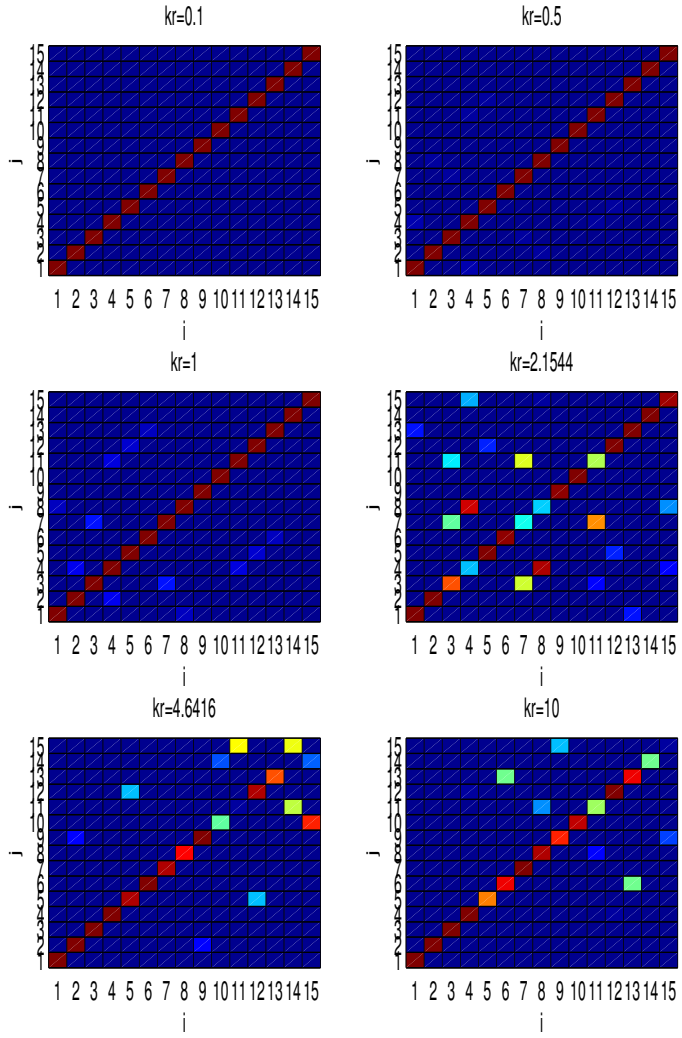


Figure 4.14: Cylinder $\frac{R}{L} = \frac{1}{2}$. Singular vectors $\boldsymbol{V}$ at several frequencies. The color indicates a scale from 0 (blue) to 1 (red) and the indices stand for the i-th column and j-th row of $\boldsymbol{V}$.

4.4 Discussion

In this chapter, a method for the modal analysis of general rotational-symmetric array geometries was presented. The method is based on the SVD of the scattering response of a rigid body due to a continuous incident plane wave distribution represented by single spherical waves. The obtained singular vectors and values can be interpreted as physical surface modes (array modes and mode strength) similar to functions known from classical acoustics.

Two examples were presented. For the spherical array, it was found that the method yields at low frequencies array modes and modal strengths corresponding to the spherical wave functions. In case of the cylinders, a similar behavior of the modes is observable but dependent on the dimensions of the cylinders the array modes are distorted versions of the spherical ones.

In general, in all cases real-valued vectors (or at least constant phase vectors) could be found and the modes are approximately frequency independent up to $k \approx 1$. Above this frequency the SVD starts to mix the singular functions because the singular values become more uniform (less degenerative). A joint SVD was applied to a set of scattering matrices $\boldsymbol{P}$ at different frequencies in between $k = 0.1 - 10$. Basically singular vectors equivalent to the ones of low frequencies can be found (not shown here). However, as can be seen in Fig. 4.15, the singular values resulting from the diagonalization using the joint singular vectors are not diagonal at no frequency (shown for sphere only). Using a joint diagonalization for frequencies below $k \approx 1$ yields better results (not shown either). This needs further investigation.

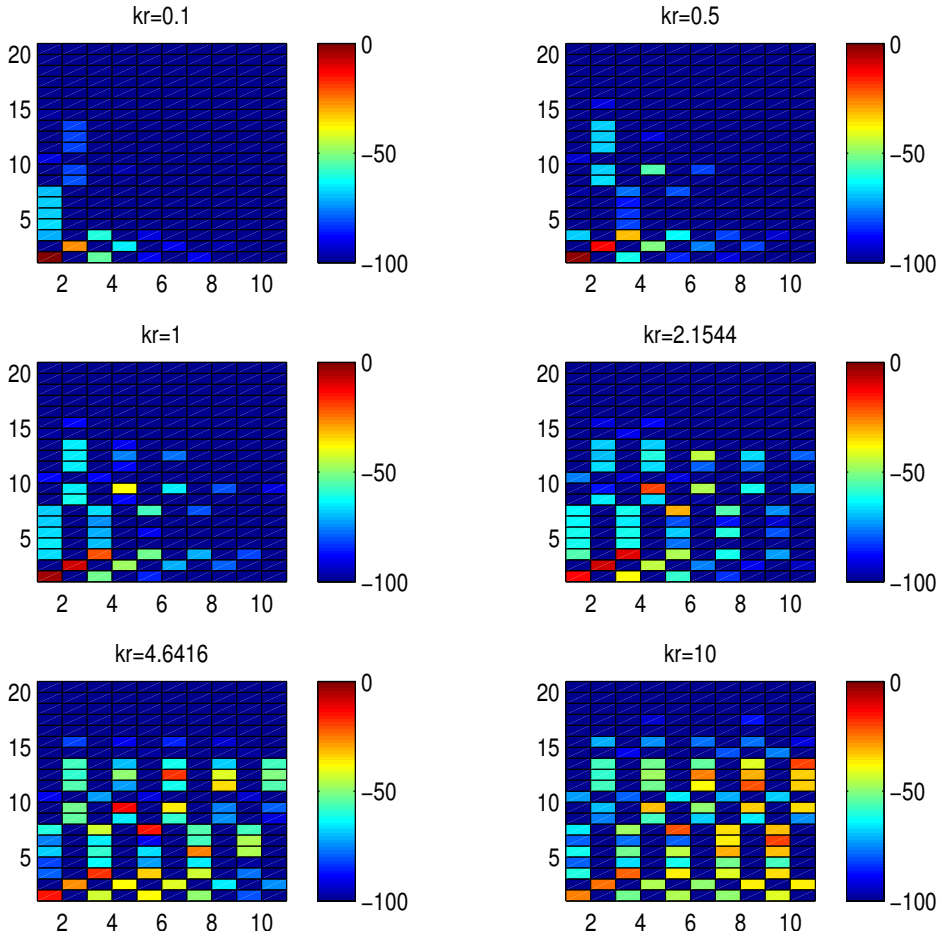


Figure 4.15: Sphere. Evaluation of the joint singular vectors. Plots $\boldsymbol{U}^{\mathrm{H}}\boldsymbol{P}\boldsymbol{V}$ for several frequencies. The joint SVD was done for $kr = 0.1 - 10$ using 12 matrices $\boldsymbol{P}$.

Chapter 5

Spatial Resolution of Cylindrical Microphone Arrays

This chapter basically reprints a publication that evolved out of the work during this thesis and was presented at an international conference [KPZ12]. The paper was written together with co-authors, Hannes Pomberger and Franz Zotter.

5.1 Introduction

Compact microphone arrays are used for sound field analysis (source localization, source identification), spatial sound recording, spatial filtering of sound (beamforming) and can be found in various applications from speech recognition to room acoustical measurements. Especially compact spherical microphone arrays received special attention over the last decade because of the uniform treatment of all directions which is crucial for the capture and reproduction of 3D acoustical scenes, cf. [ME02, AW02, Raf05]. However, in some given acoustical scenes the sound sources can be constrained only to a certain area, letting spherical arrays seem redundant. For that purpose hemispherical arrays have been investigated, see [LD05], and also circular arrays mounted on a rigid cylinder, cd. [ZDG10, TK06].

Fig. 5.1 shows different rigid shapes for microphone array geometries. The sound pressure distribution is assumed to be available on the horizontal ring in Fig. 5.1(a), on a ribbon around the horizon in Fig. 5.1(b) or on the full array Fig. 5.1(c). As this pressure distribution is the basis of array signal processing, it is simulated and used in order to compare the different resolution properties of these array types. Correlations of the pressure distributions due to different plane waves carry information about the spatial

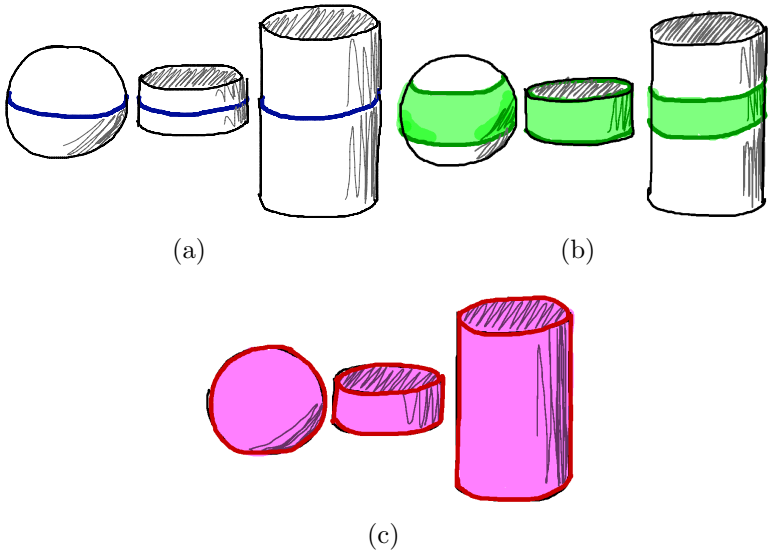


Figure 5.1: Different array shapes whose resolution properties are to be estimated: (a) ring arrays on a sphere and cylinders of different lengths, (b) ribbon arrays on a sphere and cylinders of different lengths., and (c) the entire shape used as array

resolution. We propose a method to find the resolution limits by investigating the correlation matrices of paired plane waves. The determinant of these correlation matrices measures the discriminability and is used to indicate difference angles above which two plane waves can be distinguished.

5.2 Analysis of Spatial Resolution

The scattering response for a rigid scatterer due to an incoming sound field p^I can be computed using the BEM (Ch. 3). The term p^I describes the free field sound pressure on the boundary and is expressed by

$$p^I = e^{\mathrm{i}\,k\,(x\,\cos\varphi_0\,\sin\vartheta_0 + y\,\sin\varphi_0\,\sin\vartheta_0 + z\,\sin\vartheta_0)} \tag{5.1}$$

for a plane wave impinging from φ_0, ϑ_0. The sound pressure distribution for the array design in response to any plane wave is calculated in this way. In order to evaluate the horizontal and vertical resolution as illustrated in Fig. 5.2, a set of 2 plane waves are assumed to form the matrix of quasi continuous sound pressure samples $\boldsymbol{P^I} = [\boldsymbol{p^I}(\varphi_1, \vartheta_1),\ \boldsymbol{p^I}(\varphi_2, \vartheta_2)]$. For solutions obtained with BEM, the corresponding surface sound pressure is calculated

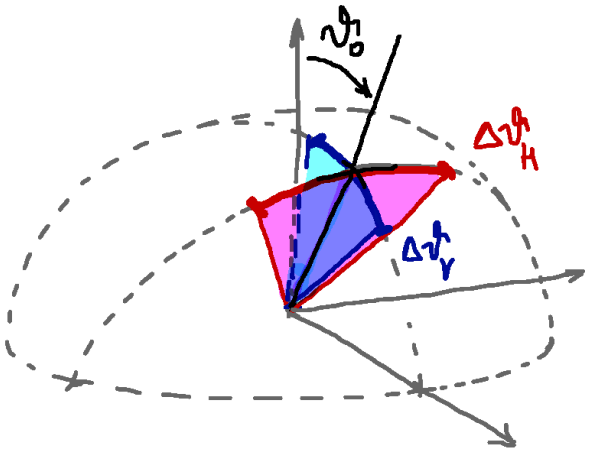


Figure 5.2: Geometry of a "vertical" and "horizontal" resolution angle with regard to a reference zenith angle ϑ_0.

according to the equation

$$\boldsymbol{P} = (\boldsymbol{H} - \boldsymbol{C})^{-1}\boldsymbol{P^I}. \tag{5.2}$$

One of our particular interests is to find out how the resolution changes with the elevation angle if a cylindrical array is used, in comparison with a spherical array that offers a uniform resolution. Let's assume a set of two plane waves from $\varphi = 0$, centered around the zenith angle ϑ_0 and separated by a space of $\Delta\vartheta$, i.e. $\boldsymbol{P^I} = [\boldsymbol{p^I}(\vartheta_0 - \Delta\vartheta/2), \boldsymbol{p^I}(\vartheta_0 + \Delta\vartheta/2)]$; another pair of plane waves that is 90° rotated with respect to ϑ_0 is used to determine the "horizontal" resolution.

The correlation of the two plane waves with regard to their surface sound pressure $\boldsymbol{P}$ obtained by Eq. (5.2) gives us a 2×2 matrix

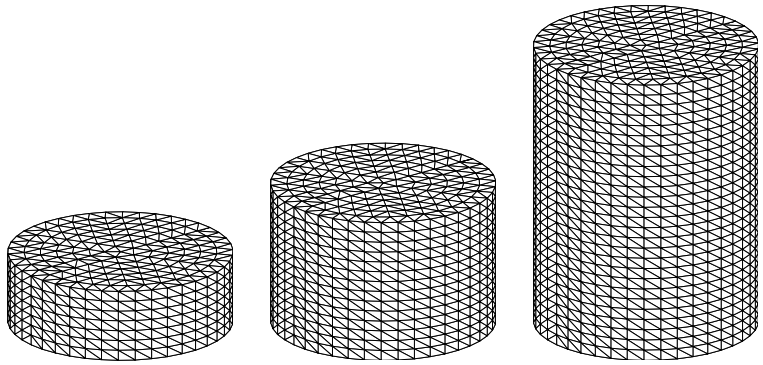
$$\boldsymbol{R}(\vartheta_0, \Delta\vartheta) = \boldsymbol{P}^{\mathrm{H}}\boldsymbol{P} = \begin{pmatrix} \boldsymbol{p}_1^{\mathrm{H}}\boldsymbol{p}_1 & \boldsymbol{p}_1^{\mathrm{H}}\boldsymbol{p}_2 \\ \boldsymbol{p}_2^{\mathrm{H}}\boldsymbol{p}_1 & \boldsymbol{p}_2^{\mathrm{H}}\boldsymbol{p}_2 \end{pmatrix} = \begin{pmatrix} r_{11} & r_{12} \\ r_{12}^* & r_{22} \end{pmatrix}. \tag{5.3}$$

In order to distinguish between these two plane waves, the determinant

$$|\boldsymbol{R}(\vartheta_0, \Delta\vartheta)| = r_{11}r_{22} - r_{12}^* r_{12} \tag{5.4}$$

must be big enough, i.e. $\sqrt{|\boldsymbol{R}(\vartheta_0, \Delta\vartheta)|} \geq \mathrm{R_{th}}$. Herein, $\mathrm{R_{th}}$ is a threshold proportional to the squared sound pressure. This measure can be seen to reflect the acoustic properties of a certain geometry concerning the discrimination capabilities of different sound pressure distributions due to different incidence directions.

5.3 Simulation Results



(a) R=1, L=0.5 (b) R=1, L=1 (c) R=1, L=2

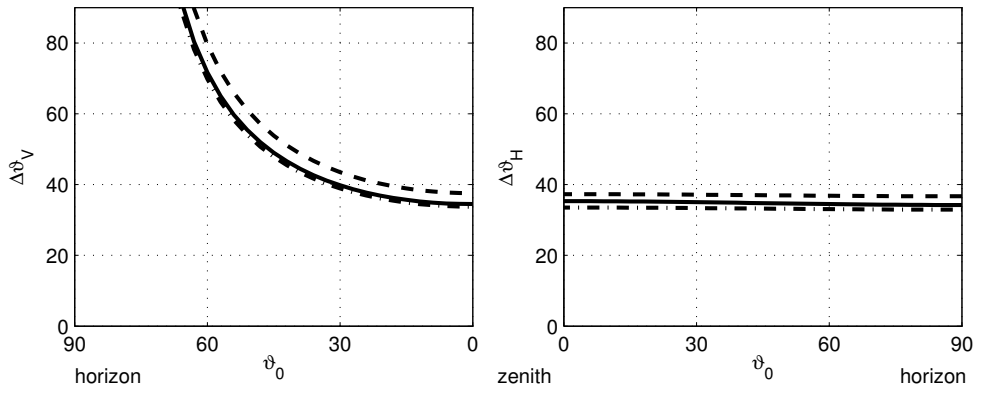
Figure 5.3: Cylinders models for BEM at different ratios (2:1, 1:1, 1:2) between height and diameter.

3 The three different configurations shown in Fig. 5.3 (ring, ribbon, whole surface array) are simulated assuming a dense enough sampling, i.e. the absence of spatial aliasing. For the ribbon-shaped array surface, a fixed height of ± 0.5R is used. Fig. 5.4-5.6 show the spatial resolution that was calculated using Eqs. 5.3 and 5.4 choosing a threshold of $R_{th} \geq 0.5$ and two different wavenumbers $k = 0.4$ and $k = 6$. All diagrams are divided into a left half depicting the "vertical" resolution and a right half depicting the "horizontal" resolution.

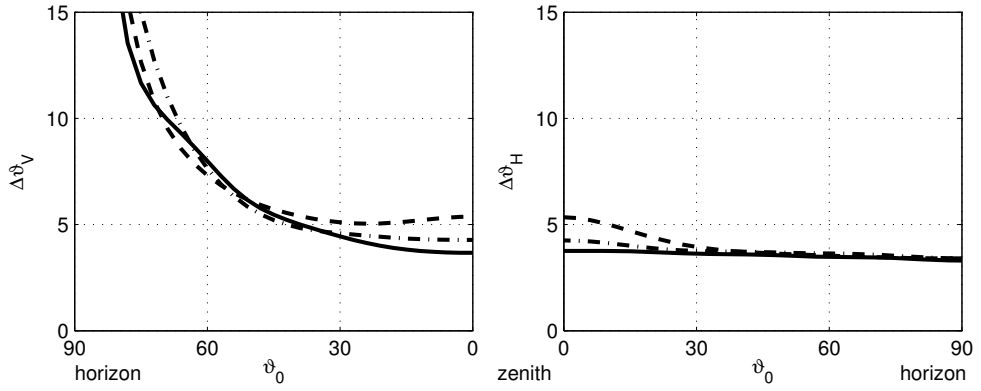
Fig. 5.4 shows that ring arrays on the different scatterers cannot resolve waves that are symmetric around the equatorial plane $\vartheta_0 = \pi/2$. This accounts for the typical half space confusion of symmetrical planar arrays. The resolution improves for directions closer to the zenith and nadir, where it is similar to the approximately constant horizontal resolution. Naturally, the resolution is better for the higher wavenumber where one or more wavelengths are sampled by the array. Overall, the resolution of all cylindrical scatterers is similar to the one of the sphere, except for ϑ_0 around zenith or nadir, where it is slightly smaller.

Fig. 5.5 plots the resolution of ribbon-shaped arrays on the different scatterers. The best horizontal and vertical resolution is similar, and the resolution around the equatorial plane $\vartheta_0 = \pi/2$ strongly improves as the array extends in three dimensional. Again, cylindrical scatterers seem slightly inferior to a spherical one.

Fig. 5.6 shows the spatial resolution for an active array aperture covering the entire surface of the scatterer. As expected, the full-sampled sphere yields



(a) kR = 0.4



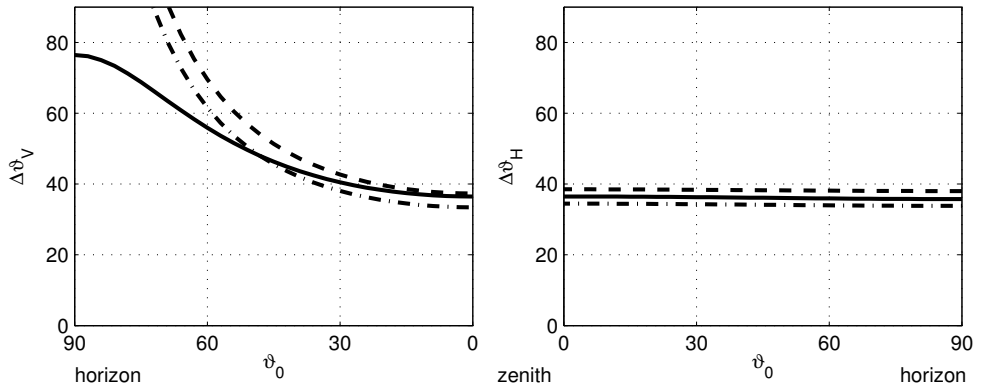
(b) kR = 6.0155

Figure 5.4: Spatial resolution for a ring array on different bodies, cf. Fig. **??**. The solid line represents a sphere, the dashed line a cylinder with $R = 1, L = 0.5$ and the dash-dotted line a cylinder with $R = 1, L = 2$.

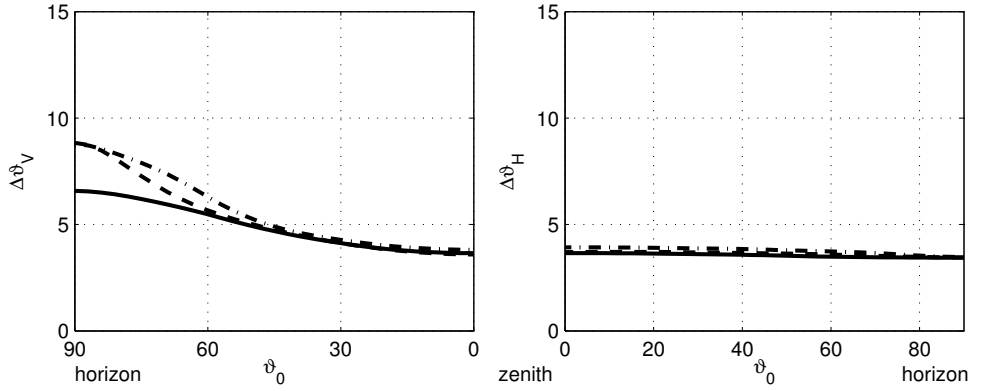
constant resolution in all directions, whereas it is only constant horizontally for the cylinders. The vertical resolution of long cylindrical scatterers with an array spread on the entire surface is naturally better around $\vartheta_0 = \pi/2$ than for a sphere of the same radius.

5.4 Discussion

We proposed a horizontal and vertical resolution measure to evaluate ring and ribbon-shaped array apertures on cylindrical scatterers. The observation was mostly based on numerical simulations, and analytic formulations were included for the cases of a rigid sphere and the infinite cylinder.

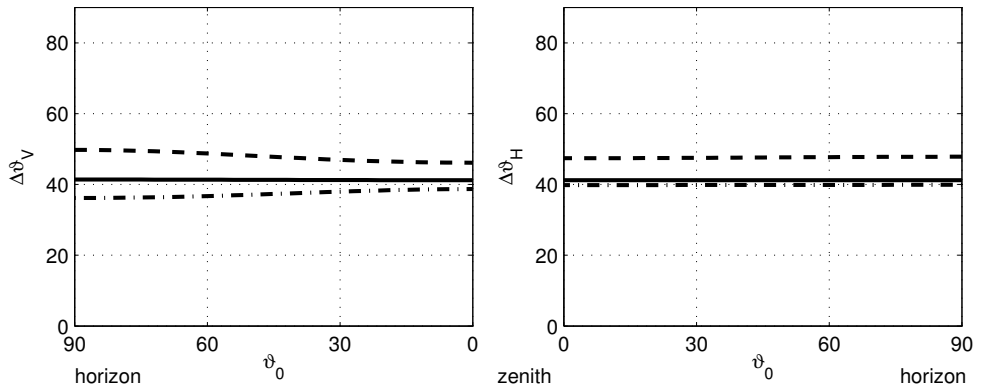


(a) kR = 0.4

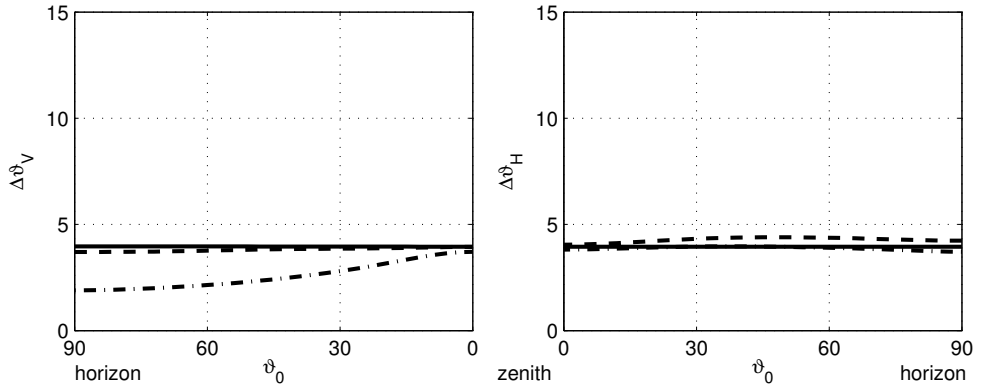


(b) kR = 6.0155

Figure 5.5: Spatial resolution for a ribbon array on different bodies, cf. Fig. **??**. The solid line represents a sphere, the dashed line a cylinder with $R = 1, L = 0.5$ and the dash-dotted line a cylinder with $R = 1, L = 2$.



(a) kR = 0.4



(b) kR = 6.0155

Figure 5.6: Spatial resolution for an array fully sampling different bodies, cf. Fig. **??**. The solid line represents a sphere, the dashed line a cylinder with R=1, L=0.5 and the dash-dotted line a cylinder with R=1,L=2.

Concluding, the horizontal resolution does not vary much for arrays on different scatterers, even at different zenith angles ϑ_0. It seems that the vertical resolution is merely affected around $\vartheta = \pi/2$ and the difference is determined by the height of the effective array aperture. Hence, only the cylinder that is twice as high as wide clearly outperforms a spherical array in its vertical resolution around the horizontal plane.

Exploiting the scattering off a cylinder to build microphone arrays does not seem to yield a substantially different spatial resolution compared to the sphere and should be further investigated because in general cylindrical arrays are easier to realize practically.

Chapter 6

Conclusions

This work is concerned with microphone arrays and the influence of different array shapes on the involved signal processing and the spatial performance. Basic analytic and numeric tools were introduced and used to analyze spherically and cylindrically shaped rigid microphone arrays. This work focussed on the acoustic front-end of microphone arrays and not the signal processing as such.

The main part of this thesis introduced a method to compute sets of basis functions for the decomposition of signals measured with the array. The method is based on the singular value decomposition of a scattering operator computed using the BEM. The difference to the techniques presented in literature is that the scattering operator includes a spherical wave transform and the corresponding inverse problem tries to reconstruct the expansion coefficients from the measured signals rather then the source strength or density.

The array modes for a spherical shaped array are well-know from acoustic literature and correspond to the spherical harmonics. These functions are frequency independent and real-valued which simplifies the subsequent signal processing severely. The question was raised if we can find functions with similar properties also for other shapes and the cylinder was used as an example. For low frequencies, below $kr \approx 1$ such functions could be found. Above that frequency the SVD is not unique anymore. The try to diagonalize the operators for several frequencies did not directly provide good results, which may be due to numerical issues. This need further investigations. Nevertheless, it can be stated that uniform functions for low frequencies can be provided using this method. At higher frequencies the basis functions are dependent on the frequency, however, the overall complexity of the signal processing can be reduced.

The second major part of this thesis was already presented in a publi-

cation and was reprinted with a few adjustments. The spatial resolution of different array shapes was investigated by looking at the correlation of the array response to incident plane wave of varying direction. Again, this is not concerned with properties of the signal processing but with the basic acoustic properties of a rigid array. The resolution of different cylindrical array configurations were not found to be of essential difference compared to equivalent spherical arrays layouts. This indicates that cylindrical arrays yield a similar performance as spherical arrays but may have the advantage of simpler practical realization.

Appendix A

Fourier Analysis

A.1 Fourier Series

Using a Fourier series any kind of periodic function defined in an interval $a \leq x \leq b$ can be represented by an infinite sum of cosine and sine functions. It is given by

$$f(x) = a_0 + \sum_{n=1}^{\infty} \big(a_n \cos nx + b_n \sin nx\big), \tag{A.1}$$

where $f(x)$ is a 2π-periodic function and a_n and b_n are the Fourier coefficients. The coefficients can be computed by the Euler formulas

$$\begin{aligned} a_0 &= \frac{1}{2\pi} \int_{-\pi}^{\pi} f(x)\ dx\ , \\ a_n &= \frac{1}{\pi} \int_{-\pi}^{\pi} f(x) \cos nx\ dx\ , \\ b_n &= \frac{1}{\pi} \int_{-\pi}^{\pi} f(x) \sin nx\ dx. \end{aligned} \tag{A.2}$$

The Fourier series simplifies some mathematical relations and made it possible to solve the wave equation in cartesian coordinates. The trigonometric functions, e.g., can be seen as the fundamental modes of vibration of a string.

A.2 Generalized Fourier Series

The Fourier series is an orthogonal expansion which is based on the trigonometric system. This can be generalized by using any kind of orthogonal

system.

May $y_0, y_1, y_2, \ldots$ be a set of orthogonal functions on an interval $a \leq x \leq b$ defined by

$$(y_k, y_i) = \int_a^b w(x) y_k(x) y_i(x)\, dx = \delta_{ki} = \begin{cases} 0 & \text{if} \quad k \neq i \\ 1 & \text{if} \quad k = i \end{cases}, \tag{A.3}$$

where δ_{ki} is the Kronecker delta, $w(x)$ is a weighting function and the norm $||y_k||$ is given by

$$||y|| = \sqrt{(y_k, y_k)} = \sqrt{\int_a^b w(x)\, y^2(x) dx}\,. \tag{A.4}$$

Then, any function $f(x)$ on the interval can be represented as

$$f(x) = \sum_{k=0}^{\infty} a_k\, y_k(x)\ , \tag{A.5}$$

where a_k are the coefficients (Fourier constants) of the orthogonal expansion (generalized Fourier series) [Kre06, Sec. 11.6].

The orthogonality allows for deriving a generalized form of Euler's formulas for obtaining the coefficients. This is done by multiplying both sides of Eq. A.5 by y_i and integrate from a to b (omitting the variable x)

$$\int_a^b f\ y_i\ dx = \int_a^b \Big(\sum_{k=0}^{\infty} a_k y_k \Big) y_i\ dx\ . \tag{A.6}$$

The term on the right hand side can be simplified using the orthogonality of the functions y_k (with nonzero norm),

$$\sum_{k=0}^{\infty} a_k \int_a^b y_k y_i\ dx\ = \sum_{k=0}^{\infty} a_k\, \delta_{ki}\, ||y_i||^2 = a_i\, ||y_i||^2 \quad \text{(for k=i)}. \tag{A.7}$$

Finally, the Fourier coefficients can be obtained by

$$a_k = \frac{1}{||y_k||^2} \int_a^b f(x)\ y_k(x)\ dx\ . \tag{A.8}$$

Completeness A set of orthogonal function is complete if the mean square error converges to zero,

$$\lim_{k\to\infty} ||f(x) - \sum_{k=0}^{\infty} a_k y_k(x)||^2 = 0\,. \tag{A.9}$$

Further, a finite set of orthogonal functions is also said complete if the mean square error is smaller than a threshold $\epsilon > 0$ [Kre06, Ch. 5.8],

$$||f(x) - \sum_{k=0}^{K} a_k y_k(x)||^2 < \epsilon\,. \tag{A.10}$$

where K is the number of orthogonal functions. In this case Bessel's inequality holds

$$\sum_{k=0}^{K} a_k \leq ||f(x)||^2\,. \tag{A.11}$$

If a set of orthogonal functions is infinite, this becomes Parseval's theorem [Wei12]

$$\sum_{k=0}^{\infty} a_k^2 = ||f(x)||^2 = \int_a^b f(x)^2\, dx\,. \tag{A.12}$$

Examples of general Fourier series are the Fourier-Legendre series and the Fourier-Bessel series [Kre06, Sec. 11.6].

A.3 Fourier Transform

The Fourier series is applicable on periodic functions only. An extension of this is to generalize the Fourier series by using any kind of orthogonal basis defined on a finite interval only. A second extension is found when the Fourier series is extended to nonperiodic functions. This leads to the Fourier integrals and the Fourier transform. In general, an integral transform changes a function into a new function that is dependent on another variable. It is an important tool for solving differential- and integral equations, because differentiations are converted into algebraic operations.

The Fourier transform shown here is a complex transform, in contrast to the Fourier cosine or sine transforms. It is derived from the complex form of the Fourier integral which is the extension of the Fourier series to non-periodic functions (see [Kre06, Sec. 11.9]). As in the framework of array signal processing, both, the spatial Fourier transform and the temporal Fourier

transform are of interest, they shell both be defined here. The temporal Fourier transform $F(\omega)$ of a time-domain function $f(t)$ is given by

$$F(\omega) = \int_{-\infty}^{\infty} f(t) e^{-i\omega t} dt \ , \tag{A.13}$$

and it's inverse

$$f(t) = \frac{1}{2\pi} \int_{-\infty}^{\infty} F(\omega) e^{i\omega t} dt \ , \tag{A.14}$$

where $\omega = 2\pi f$ is the radial frequency. It yields the relation between a time-domain function and it's frequency-domain representation.

The spatial Fourier transform $F(k_x)$ of a spatial function $f(x)$ is given by

$$F(k_x) = \int_{-\infty}^{\infty} f(x) e^{ik_x x} dx \ , \tag{A.15}$$

and it's inverse

$$f(x) = \frac{1}{2\pi} \int_{-\infty}^{\infty} F(k_x) e^{-ik_x x} dx \ , \tag{A.16}$$

where $k_x = \frac{\omega}{c} = \frac{2\pi}{\lambda}$ is the wave number with c the speed of sound and λ the wave-length. This yields a relation between a spatial function and it's angular spectrum [Wil99, Sec. 2.9].

Appendix B

Special Functions

B.1 Bessel Functions

The Bessel functions of first and second kind, $J_n(kr)$ and $Y_n(kr)$, are the solutions to Bessel's equation (Eq. 2.20) which arises from the separation of variables of the Helmholtz equation in cylindrical coordinates [Wil99]. They state the standing wave solutions. Traveling wave solutions can be achieved by combining both functions which yields the Hankel functions of first and second kind (with time dependence $e^{i\omega t}$)

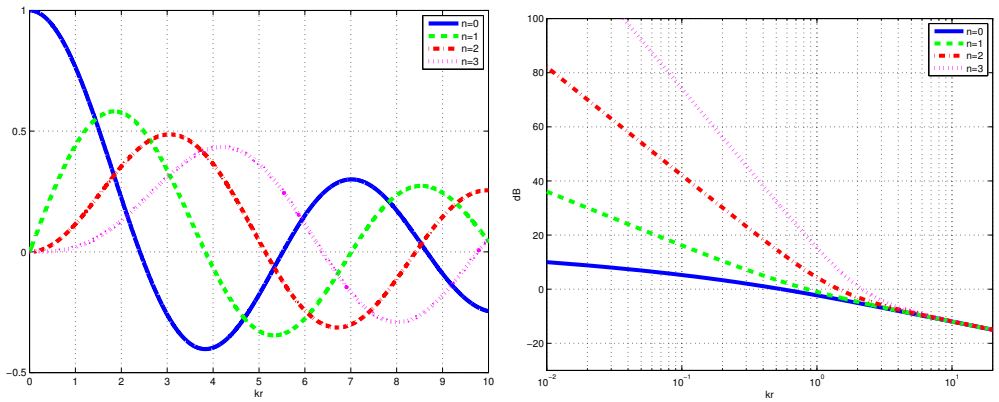
$$\begin{aligned} H_n^{(1)}(kr) &= J_n(kr) - iY_n(kr)\,, \\ H_n^{(2)}(kr) &= J_n(kr) + iY_n(kr)\,. \end{aligned} \tag{B.1}$$

Equivalently, the spherical Bessel functions of first and second kind are the standing wave solutions of spherical Bessel's equation (Eq. 2.26) which originates from the separation of variables of the Helmholtz equation in spherical coordinates. Again, traveling wave solutions are achieved by composing the spherical Bessel functions in the same way as before.

As remarked in [Zot09] not all solutions are physical and thus some solutions have to be omitted. Figure B.1 depicts the feasible cylindrical radial solutions and Fig. B.2 depicts the feasible spherical radial solutions.

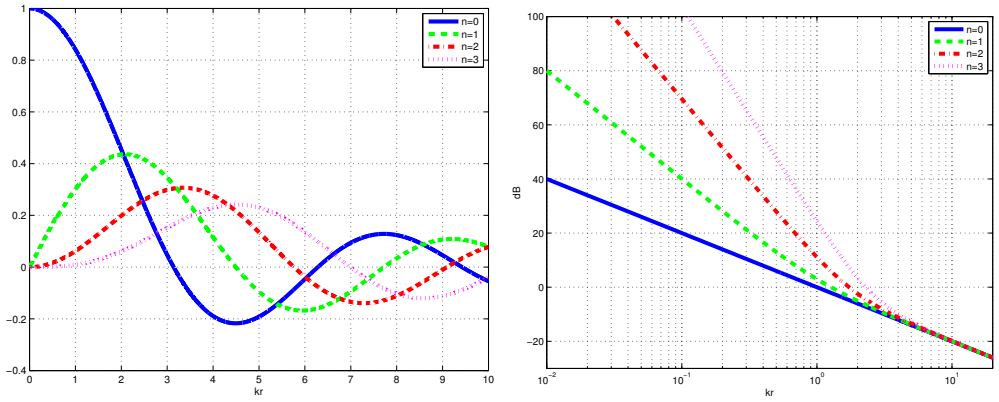
B.2 Associated Legendre Functions

The separation of variables of the Helmholtz equation in spherical coordinates yield the associated Legendre equation (Eq. 2.26) for the zenith coordinate ϑ. The solution yields the associated Legendre function of first and second kind, $P_n^m(\cos\vartheta)$ and $Q_n^m(\cos\vartheta)$, where the functions of second kind are usually



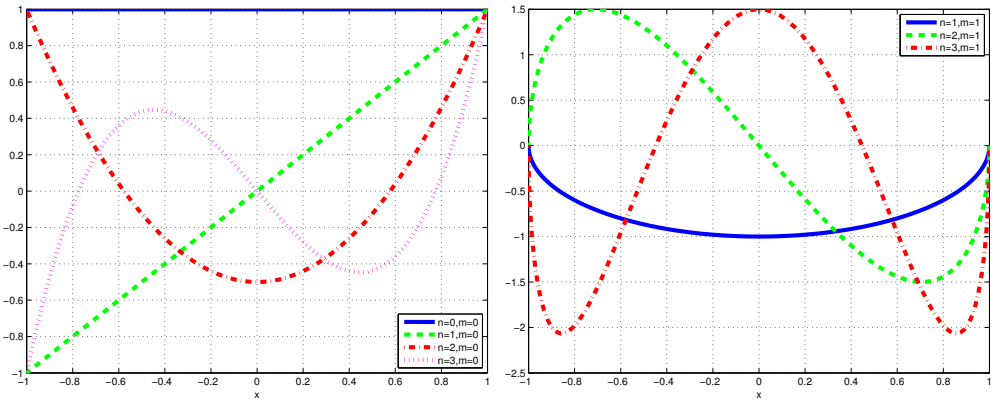
(a) (b)

Figure B.1: Bessel function of first kind (a) and Hankel function of second kind (b).



(a) (b)

Figure B.2: Spherical Bessel function of first kind (a) and spherical Hankel function of second kind (b).



(a) (b)

Figure B.3: Associated Legendre function up to order 3 for m=0 (a) and m=1 (b).

discarded because they have singularities at the poles. However they have to be used in the solutions of the Helmholtz equation on prolate and oblate spheroidal coordinates [Wei12]. Fig. B.3 depicts the associated Legendre functions of first kind.

B.3 Spherical Harmonics

The angular solutions of the Helmholtz equation in spherical coordinates are usually combined to yield the so called spherical harmonics Y_n^m. The real valued spherical harmonics are defined as

$$Y_n^m(\varphi,\vartheta) = N_n^{|m|} P_n^{|m|}(\cos\vartheta) \begin{cases} \cos(m\varphi) & \text{, for } m > 0 \\ \sin(m\varphi) & \text{, for } m \leq 0 \end{cases}, \tag{B.2}$$

where N_n^m is a normalization constant given by

$$N_n^m = (-1)^m \sqrt{\frac{(2n+1)(2-\delta_m)}{4\pi} \frac{(n-|m|)!}{(n+|m|)!}}, \tag{B.3}$$

and $P_n^{|m|}$ are the associated Legendre functions. The spherical harmonics form a complete set of orthonormal functions

$$\int_0^{2\pi} \int_0^{\pi} Y_n^m(\varphi,\vartheta) Y_{n'}^{m'}(\varphi,\vartheta) \sin\vartheta d\vartheta d\phi = \delta_{nn'}\delta_{mm'} \tag{B.4}$$

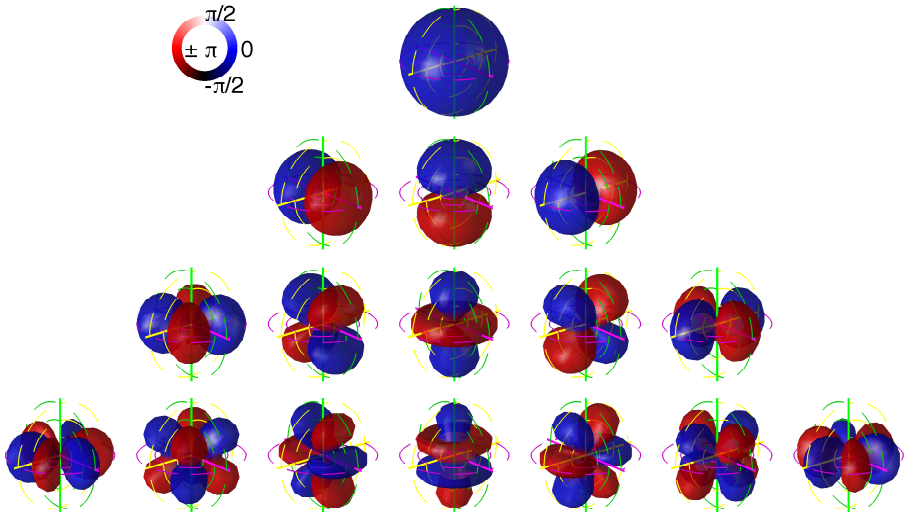


Figure B.4: Plot of the spherical harmonics up to order 3.

where $\delta_{nn'}$ is the Kronecker delta given by

$$\delta_{ij} = \begin{cases} 0 & \text{, for } i \neq j \\ 1 & \text{, for } i = j \end{cases} . \tag{B.5}$$

The orthogonality means that any kind of function $f(\varphi, \vartheta)$ defined on a sphere can be expanded using the spherical harmonics

$$f(\varphi, \vartheta) = \sum_{n=0}^{\infty} \sum_{m=-n}^{n} a_{nm} Y_n^m(\varphi, \vartheta) \,, \tag{B.6}$$

where a_{nm} are the coefficients of the expansion given by

$$a_{nm} = \int_0^{2\pi} \int_0^{\pi} f(\varphi, \vartheta)\, Y_n^m(\varphi, \vartheta) \sin\vartheta d\vartheta d\phi \,. \tag{B.7}$$

In case only the rotational symmetric harmonics (zonal harmonics) are of interest, Eq. B.2 reduces to [Wil99]

$$Y_n^0(\varphi, \vartheta) = \sqrt{\frac{2n+1}{4\pi}} P_n(\cos\vartheta) \,, \tag{B.8}$$

where P_n are the Legendre polynomials. Figure B.4 depicts the spherical harmonics up to order 3.

Appendix C

Beamforming as an Inverse Problem

The sound field due to a source distribution was represented as an integral operator in chapter 4. The main questions were concerned with the decomposition of this operator. However, the purpose of using microphone arrays is to reconstruct the incoming sound field or to focus only on a certain area in space. This problem can be formulated as an inverse problem [NE93, Faz10]. The discretely measured sound pressure due to an irradiating sound field can be written as

$$\boldsymbol{p} = \boldsymbol{P}\boldsymbol{\varphi} \tag{C.1}$$

where $\boldsymbol{P}$ is a matrix representing transfer functions, $\boldsymbol{p}$ is the vector of measured sound pressures and $\boldsymbol{\varphi}$ is the source density or source strength. $\boldsymbol{P}$ is acting from the source space S_0 and the receiver space S. The reconstruction of the sources demands a matrix inversion

$$\boldsymbol{\varphi} = \boldsymbol{P}^{-1}\boldsymbol{p}\,. \tag{C.2}$$

This inversion can be done by representing $\boldsymbol{P}$ using the SVD

$$\boldsymbol{P} = \boldsymbol{U}\boldsymbol{\Sigma}\boldsymbol{V}^{\mathrm{H}},\ \boldsymbol{P}^{-1} = \boldsymbol{V}\boldsymbol{\Sigma}^{-1}\boldsymbol{U}^{\mathrm{H}}\,, \tag{C.3}$$

or explicitly written

$$\boldsymbol{P} = \sum_{i=1}^{\mathrm{K}} \sigma_i \langle v_i, u_i \rangle,\ \boldsymbol{P}^{-1} = \sum_{i=1}^{\mathrm{K}} \frac{1}{\sigma_i} \langle u_i, v_i \rangle\,. \tag{C.4}$$

where K is the number of singular vectors and $\langle \cdot \rangle$ is the scalar product.

Practically the inversion of $\boldsymbol{P}$ using the SVD has to be regularized [Han87, Faz10]. The simplest way is to truncate the singular values and set every singular value to zero that falls below a certain threshold. This yields an approximate $\varphi_{\mathbf{a}}$

$$\varphi_{\mathrm{a}} = \boldsymbol{P}_{\mathrm{a}}^{-1}\boldsymbol{p} = \boldsymbol{V}\boldsymbol{\Sigma}_{\mathrm{a}}^{-1}\boldsymbol{U}^{\mathrm{H}}\,. \tag{C.5}$$

The goal is to make the error as small as possible, $||\boldsymbol{p} - \boldsymbol{p}_{\mathrm{a}}|| = 0$, which leads to

$$\begin{aligned} \boldsymbol{P}_{\mathrm{a}}\boldsymbol{\varphi}_{\mathrm{a}} &= \boldsymbol{P}\boldsymbol{\varphi}\,, \\ \boldsymbol{\varphi}_{\mathrm{a}} &= \boldsymbol{P}_{\mathrm{a}}^{-1}\boldsymbol{P}\boldsymbol{\varphi}\,, \\ \boldsymbol{\varphi}_{\mathrm{a}} &= \boldsymbol{V}\boldsymbol{\Sigma}_{\mathrm{a}}^{-1}\underbrace{\boldsymbol{U}^{\mathrm{H}}\boldsymbol{U}}_{\boldsymbol{I}}\boldsymbol{\Sigma}\boldsymbol{V}^{\mathrm{H}}\,\boldsymbol{\varphi}\,. \end{aligned} \tag{C.6}$$

Setting $\boldsymbol{\varphi}$ to be driving only one source direction, the expression $\boldsymbol{V}\boldsymbol{\Sigma}_{\mathrm{a}}^{-1}\boldsymbol{\Sigma}\boldsymbol{V}^{\mathrm{H}}$ can be seen as a beamforming operation where the term $\boldsymbol{\Sigma}_{\mathrm{a}}^{-1}\Sigma$ states a loss of information.

Appendix D

Modal Analysis of Free-Field Radiators

D.1 The Radiation Problem

The radiated or scattered[1] sound field from sound sources in an arbitrarily shaped region V with surface S can be represented in the free-field using Green's functions satisfying the homogeneous Neumann boundary condition on the surface of the body. The Green's function can be seen as a point source placed on an otherwise rigid body. This, so called Neumann Green's function $G_{\mathrm{N}}(\boldsymbol{x}|\boldsymbol{y})$, satisfies the following set of equations [Wil99]:

$$\begin{cases} (\Delta + k^2)G_{\mathrm{N}}(\boldsymbol{x}|\boldsymbol{y}) = & -\delta(\boldsymbol{x}-\boldsymbol{y}),\, \boldsymbol{x} \in \mathbb{R}^3, \\ \nabla G_{\mathrm{N}}(\boldsymbol{x}|\boldsymbol{y}) = & 0\,,\, \boldsymbol{y} \in S\,, \\ \lim\limits_{r\to\infty} G_{\mathrm{N}}(\boldsymbol{x}|\boldsymbol{y}) = & 0\,, \end{cases} \tag{D.1}$$

where $\boldsymbol{x} = (x_x, y_x, z_x)$ is a coordinate vector anywhere in the field and $\boldsymbol{y} = (x_y, y_y, z_y)$ is a coordinate vector on the surface S. Using Neumann Green's function in the HIE (Eq. 2.15), it becomes

$$C(\boldsymbol{x})p(\boldsymbol{x}) = \mathrm{i}\rho_0\omega \iint_S v_{\mathrm{n}}(\boldsymbol{y})G_{\mathrm{N}}(\boldsymbol{x}|\boldsymbol{y})\,\mathrm{d}S(\boldsymbol{y}), \tag{D.2}$$

where ρ_0 is the air density and v_{n} is the normal particle velocity defined by $v_{\mathrm{n}} = v \cdot \mathbf{n}_{\mathbf{y}}$ with $\mathbf{n}_{\mathbf{y}}$ the normal vector to S. Eq. D.2 states that the sound pressure anywhere in the field can be expressed by a superposition of continuously distributed point sources placed on a rigid boundary S knowing the

[1] Due to the principle of acoustic reciprocity the radiated and the scattered sound field are equal.

normal particle velocity on the surface only. Because the particle velocity on a boundary is explicitly related to the sound pressure, this integral equation is similar to Rayleigh's integral formulas [VW04]. Further it can be seen as a transfer impedance operator relating the sound pressure in the field and the particle velocity on the boundary S [NK01].

This relation is dependent on frequency and the geometry. Changing the geometry of the source or the field boundary, changes the Neumann Green's function and also changing the frequency influences the outcome of the integration.

D.1.1 Singular Functions of the Radiation Operator

Using operator notation, Eq. D.2 can be written as

$$p(\boldsymbol{x}) = (\mathcal{G}_{\mathcal{N}}\, v_{\mathrm{n}})(\boldsymbol{x}), \tag{D.3}$$

where $\mathcal{G}_{\mathcal{N}}$ is the operator representing the integral operation of Eq. D.2 defined as $\mathcal{G}_{\mathcal{N}} : S \to S_0$ where S_0 is the space of the observation points in the far-field. The singular system or spectral decomposition of this radiation operator is given by

$$\mathcal{G}_{\mathcal{N}} = \sum_{j=1}^{\infty} u_j(\boldsymbol{x})\, \sigma_j\, v_j(\boldsymbol{y}) \tag{D.4}$$

where σ_j are the singular values and $u_j(\boldsymbol{x})$ and $v_j(\boldsymbol{y})$ are the left and right singular functions, respectively [CK98] [Bor90], [Faz10, Ch. 3]. Eq. D.4 is analogous to the SVD of a matrix. The singular functions form two sets of orthogonal functions and the singular values relate the singular functions to each other. Using the spectral decomposition in Eq. D.3 it becomes

$$p(\boldsymbol{x}) = (\mathcal{G}_{\mathcal{N}}\, v_{\mathrm{n}})(\boldsymbol{x}) = \sum_{n=1}^{\infty} u_j(\boldsymbol{x})\, \sigma_j\, \langle v_j | v_{\mathrm{n}} \rangle, \tag{D.5}$$

where $\langle v_j | v_{\mathrm{n}} \rangle$ is the scalar product of the velocity pattern with the singular functions of the radiator defined by

$$\langle v_j | v_{\mathrm{n}} \rangle = \int v_{\mathrm{n}}(\boldsymbol{y})\, v_j^*(\boldsymbol{y})\, \mathrm{d}\boldsymbol{y}\,, \tag{D.6}$$

where v_j^* indicates the complex conjugate.

The singular vectors are as the *acoustic radiation modes* of the radiating boundary S and the field or measurement boundary S_0 and the singular values correspond to the *radiation efficiencies* of the modes [CNC01]. Equivalentely Nelson [NK01] calls them the "source modes" and the "field modes".

D.1.2 Neumann Green's Function Matrix

The Green's function satisfying specific boundary conditions is not easy to express unless the geometry of the problem corresponds to one of the separable ones [MF53, Ch. 5]. However, using the free-field Green's function one can express the Neumann or the Dirichlet Green's function using the HIE [Wil99, VW04, NK01]. This is not exliciltly shown here. The practical way of calculating a matrix containing the single contributions of the Neuman Green's function is presented now.

The discretized version of the HIE is given by (cf. Ch. 3 for more detail)

$$\boldsymbol{C}\boldsymbol{p} = \boldsymbol{H}\boldsymbol{p} - \boldsymbol{G}\boldsymbol{p}_{\mathbf{n}}\,. \tag{D.7}$$

where $\boldsymbol{p}$ and $\boldsymbol{p}_{\mathbf{n}}$ are the sound pressure and its normal derivative in vector form and $(\boldsymbol{C}, \boldsymbol{G}, \boldsymbol{H}) \in \mathbb{R}^{\mathrm{L}\times\mathrm{L}}$ are the BEM matrices where L is the number of surface points. Now, the radiated sound field can be calculated in two steps assuming $\boldsymbol{p}_{\mathbf{n}}$ to be known. First, the sound pressure on the boundary ($\boldsymbol{x} \in S$) is expressed by

$$\boldsymbol{p}_{\boldsymbol{s}} = (\boldsymbol{H}^{(\mathrm{s})} - \boldsymbol{C}^{(\mathrm{s})})^{-1}\boldsymbol{G}^{(\mathrm{s})}\boldsymbol{p}_{\mathbf{n}}^{(\mathrm{s})}, \tag{D.8}$$

where the subscript s indicates the relations on the surface. Secondly, knowing the sound pressure and its normal derivative on the boundary S, the sound pressure exterior to the region V ($\boldsymbol{x} \in \mathbb{R}^3\backslash V$) can be written as

$$\boldsymbol{p}^{(\mathrm{f})} = \boldsymbol{H}^{(\mathrm{f})}(\boldsymbol{H}^{(\mathrm{s})} - \boldsymbol{C}^{(\mathrm{s})})^{-1}\boldsymbol{G}^{(\mathrm{s})}\boldsymbol{p}_{\mathbf{n}}^{(\mathrm{f})} - \boldsymbol{G}_{\boldsymbol{f}}\boldsymbol{p}_{\mathbf{n}}^{(\mathrm{f})}, \tag{D.9}$$

where the subscript f indicates the matrix relations from the boundary to the field and $(\boldsymbol{G}^{\mathrm{f}}, \boldsymbol{H}^{\mathrm{f}}) \in \mathbb{R}^{\mathrm{L}\times\mathrm{F}}$ where F is the number of field points. Further,

$$\boldsymbol{p}^{(\mathrm{f})} = \underbrace{\left(\boldsymbol{H}^{(\mathrm{f})}(\boldsymbol{H}^{(\mathrm{s})} - \boldsymbol{C}^{(\mathrm{s})})^{-1}\boldsymbol{G}^{(\mathrm{s})} - \boldsymbol{G}^{(\mathrm{f})}\right)}_{\boldsymbol{G}_{\mathrm{N}}}\boldsymbol{p}_{\mathbf{n}}^{(\mathrm{f})}, \tag{D.10}$$

where $\boldsymbol{G}_{\mathrm{N}}$ is the Neumann Green's function G_{N} in matrix representation. The radiation problem can be written in matrix form

$$\boldsymbol{p} = \boldsymbol{G}_{\mathrm{N}}\,\boldsymbol{v}_{\mathrm{n}}\,. \tag{D.11}$$

D.1.3 SVD of Neumann Green's Function Matrix

Using the SVD of the Neumann Green's function matrix, Eq. D.11 can be written to

$$\boldsymbol{p} = \boldsymbol{U}\boldsymbol{\Sigma}\boldsymbol{V}^{\mathbf{H}}\,\boldsymbol{v}_{\mathrm{n}} \tag{D.12}$$

where $\boldsymbol{U} \in \mathbb{R}^{\mathrm{L}\times\mathrm{L}}$ contains the left singular-vectors in columns, $\boldsymbol{V} \in \mathbb{R}^{\mathrm{F}\times\mathrm{F}}$ contains the right singular vectors and $\boldsymbol{\Sigma} \in \mathbb{R}^{\mathrm{L}\times\mathrm{F}}$ is a diagonal matrix containing the singular values. When rewriting this equation to

$$\boldsymbol{U}^{\mathrm{H}}\,\boldsymbol{p} = \boldsymbol{\Sigma}\boldsymbol{V}^{\mathbf{H}}\,\boldsymbol{v}_{\mathrm{n}}\,, \tag{D.13}$$

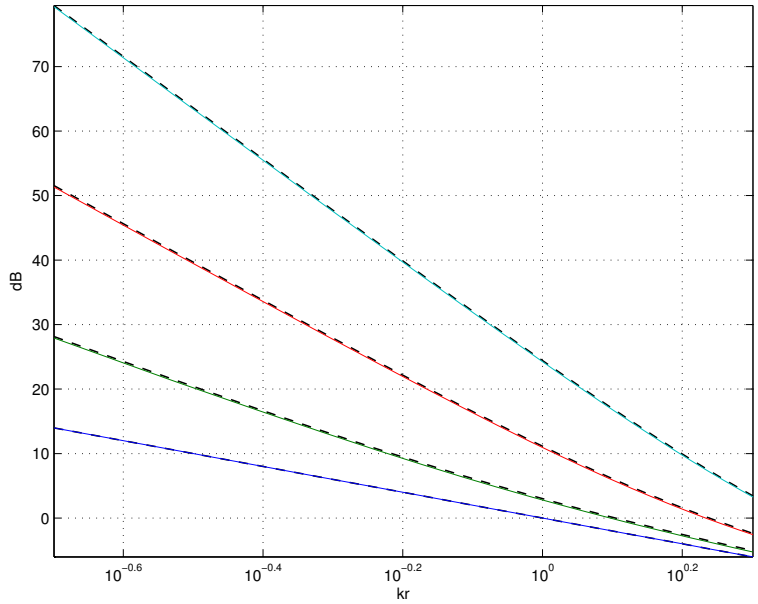
it becomes clear that the singular vectors $\boldsymbol{U}$ state a set of basis vectors for the space of $\boldsymbol{p}$ and $\boldsymbol{V}$ represents the same for the space of $\boldsymbol{v}_{\mathrm{n}}$. This indicates a correspondence of the results of the SVD and the basis functions derived for separable geometry's [NK01].

Equivalent to the singular functions from before the singular vectors are the *acoustic radiation modes* and the singular values are the corresponding *radiation efficiencies*. Again, it has to be clearly stated that the result of the SVD is dependent on the frequency and the geometric relations of the radiating surface S and the receiving surface S_0.

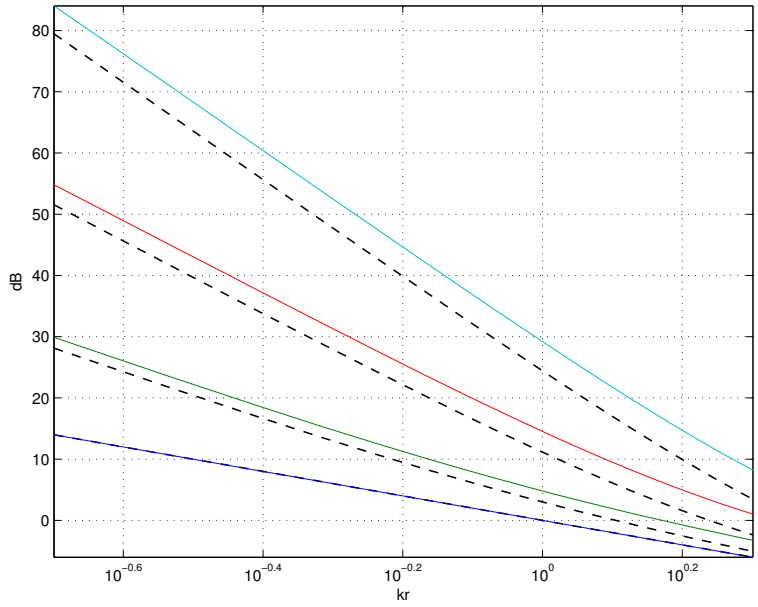
D.2 Radiation Modes for Varying Scalings

As a thorough modal analysis of a sphere and a cylinder is presented in Ch. 4 and the array modes obtained using the SVD of Green's function matrix yields equivalent modes, this is not repeated here. However, with both methods described in this thesis, a modal analysis for different scalings (distances) of the field points or the source distribution can be achieved. This is interesting because the singular values will correspond to functions representing sound propagation.

The simulations were conducted using the axisymmetric BEM formulation for $m = 0$. Fig. D.1 (a) shows the singular values over different scalings of the field points for the sphere. It can be seen that they correspond exactly to the magnitude of the spherical Hankel functions. In Fig. D.1 (b) the same simulation is shown but for a cylinder of dimensions $\frac{R}{L} = \frac{1}{1}$. It can be seen that also the cylinder follows the Hankel functions but the values for order $N > 0$ are higher.



(a)



(b)

Figure D.1: Singular values over different scalings $r = 2 - 20$. (a) Sphere, (b) Cylinder $\frac{R}{L} = \frac{1}{1}$

Bibliography

[AS64] M. Abramowitz and I.A. Stegun. *Handbook of mathematical functions with formulas, graphs, and mathematical tables*. Number v. 55, no. 1972 in Applied mathematics series. U.S. Govt. Print. Off., 1964.

[AW02] Thushara D. Abhayapala and Darren B. Ward. Theory and design of high order sound field microphones using spherical microphone array. In *Acoustics, Speech, and Signal Processing (ICASSP), 2002 IEEE International Conference on*, volume 2, pages II–1949 –II–1952, 2002.

[AW05] G.B. Arfken and H.J. Weber. *Mathematical methods for physicists*. Elsevier, 2005.

[Bee08] G. Beer. *The Boundary element method with programming - For engineers and scientists*. Springer, 2008.

[BM71] A. J. Burton and G.F. Miller. The application of integral equation methods to the numerical solution of some exterior boundary-value problems. *Proc. Roy. Soc. Lond. A.*, 323:201–210, 1971.

[Bor90] Giorgio V. Borgiotti. The power radiated by a vibrating body in an acoustic fluid and its determination from boundary measurements. *The Journal of the Acoustical Society of America*, 88(4):1884–1893, 1990.

[BW92] G. Beer and J. O. Watson. *Introduction to finite and boundary element methods for engineers*. Wiley, 1992.

[CB91] R.D. Ciskowski and C.A. Brebbia. *Boundary element methods in acoustics*. Computational Mechanics Publications, 1991.

[CC94] Kenneth A. Cunefare and M. Noelle Currey. On the exterior acoustic radiation modes of structures. *The Journal of the Acoustical Society of America*, 96(4):2302–2312, 1994.

[CH01] Vicente Cutanda Henriquez. *Numerical Transducer Modeling*. PhD thesis, Danish Acedemy of Technical Science (ATV), 2001.

[CHJ10] Vicente Cutanda Henriquez and Peter Moller Juhl. Openbem - an open source boundary element method software in acoustics. *Internoise 2010*, 2010.

[CK91] D.L. Colton and R. Kress. *Integral Equation Methods in Scattering Theory*. Pure and Applied Mathematics Series. Krieger Publishing Company, 1991.

[CK98] D.L. Colton and R. Kress. *Inverse Acoustic and Electromagnetic Scattering Theory*. Applied Mathematical Sciences. Springer, 1998.

[CNC01] Kenneth A. Cunefare and M. Noelle Currey. The radiation efficiency grouping of free-space acoustic radiation modes. *J. Acoust. Soc. Am.*, 109(1), 2001.

[CS96] Jean-François Cardoso and Antoine Souloumiac. Jacobi angles for simultaneous diagonalization. *SIAM J. Mat. Anal. Appl.*, 17(1):161–164, 1996.

[CW07] Steve; Chandler-Wilde, Simon; Langdon. Boundary element methods for acoustics, 2007.

[EJ93] S. J. Elliott and M. E. Johnson. Radiation modes and the active control of sound power. *The Journal of the Acoustical Society of America*, 94(4):2194–2204, 1993.

[Faz10] Filippo Fazi. *Sound Field Reproduction*. PhD thesis, University of Southampton, 2010.

[GD04] N.A. Gumerov and R. Duraiswami. *Fast Multipole Methods for the Helmholtz Equation in Three Dimensions*. Elsevier, 2004.

[GG06] Mathieu Guillaume and Yves Grenier. Theoretical sound field analysis. Technical report, Telecom Paris, 2006.

[Han87] P.C. Hansen. *Rank-Deficient and Discrete Ill-Posed Problems: Numerical Aspects of Linear Inversion*. Siam Monographs on Mathematical Modeling and Computation. SIAM, 1987.

[Hor09] Gen Hori. Comparison of two main approaches to joint svd. In Tülay Adali, Christian Jutten, João Romano, and Allan Barros, editors, *Independent Component Analysis and Signal Separation*, volume 5441, pages 42–49. Springer Berlin / Heidelberg, 2009.

[Jes73] M. Jessel. *Acoustique théorique*. Masson, 1973.

[Juh93] Peter M. Juhl. *The boundary element method for sound field calculations*. PhD thesis, Thechnical University of Denmark, 1993.

[KP11] T. Kolehmainen and S. Pohjolainen. Estimation of acoustic boundary impedance using bem and inverse mehtods. *International Association for Mathematics and Computers in Simulation*, 2011.

[KPZ12] Fabio Kaiser, Hannes Pomberger, and Franz Zotter. Investigations on cylindrical microphone arrays. *25th AES UK Conference in association with the 4th International Symposium on Ambisonics and Spherical Acoustics*, 2012.

[Kre06] E. Kreyszig. *Advanced engineering mathematics*. Wiley, 10th edition, 2006.

[LD05] Zhiyun Li and Ramani Duraiswami. Hemispherical microphone array for sound capture and beamforming. In *IEEE Workshop on Applications of Signal Processing to Audio and Acoustics, 2005*, 2005.

[Mar02] Stefan Marburg. Six elements per wavelength. is that enough? *Journal of Computational Acoustics*, 10(25-51), 2002.

[ME02] Jens Meyer and Gary Elko. A highly scalable spherical microphone array based on an orthonormal decomposition of the soundfield. In *Acoustics, Speech, and Signal Processing (ICASSP), 2002 IEEE International Conference on*, volume 2, pages II–1781 –II–1784, 2002.

[Mey01] Jens Meyer. Beamforming for a circular microphone array mounted on spherically shaped objects. *The Journal of the Acoustical Society of America*, 109(1):185–193, 2001.

[MF53] P.M.C. Morse and H. Feshbach. *Methods of theoretical physics*. Number v. 1 in International series in pure and applied physics. McGraw-Hill, 1953.

[MH99] Stefan Marburg and H.-J. Hardtke. A study on the acoustic boundary admittance. determinantion, results and consequences. *Engineering Analysis with Boundary Elements*, 23:737–744, 1999.

[MI86] P.M.C. Morse and K.U. Ingard. *Theoretical acoustics*. Princeton University Press, 1986.

[NE93] P. A. Nelson and S. J. Elliott. *Active control of sound*. Academic Press, 1993.

[NK01] P.A. Nelson and Y. Kahana. Spherical harmonics, singular-value decomposition and the head realated transfer function. *Journal of Sound and Vibration*, 239(4):607–637, 2001.

[PdFAH10] Alexander Mattioli Pasqual, Jose Roberto de Franca Arruda, and Phillipe Herzog. Application of acoustic radiation modes in the directivity contril by a spherical loudspeaker array. *Acta Acoustica united with Acoustica*, 96:32–42, 2010.

[Pho90] Douglas M. Photiadis. The relationship of singular value decomposition to wave-vector filtering in sound radiation problems. *The Journal of the Acoustical Society of America*, 88(2):1152–1159, 1990.

[PKM12] Herwig Peters, Nicole Kessissoglou, and Steffen Marburg. Enforcing reciprocity in numerical analysis of acoustic radiation modes and sound power evaluation. *Journal of Computational Acoustics*, 20(3), 2012.

[PM11] Alexander Mattioli Pasqual and Vincent Martin. On the acoustic radiation modes of compact regular polyhedral arrays of independent loudspeakers. *The Journal of the Acoustical Society of America*, 130(3):1325–1336, 2011.

[Raf05] B. Rafaely. Analysis and design of spherical microphone arrays. *Speech and Audio Processing, IEEE Transactions on*, 13(1):135 – 143, 2005.

[RWB07] Boaz Rafaely, Barak Weiss, and Eitan Bachmat. Spatial aliasing in spherical microphone arrays. *Signal Processing, IEEE Transactions on*, 55(3):1003 –1010, 2007.

[Sar90] Angie Sarkissian. Near-field acoustic holography for an axisymmetric geometry: A new formulation. *The Journal of the Acoustical Society of America*, 88(2):961–966, 1990.

[Sar91] Angie Sarkissian. Acoustic radiation from finite structures. *The Journal of the Acoustical Society of America*, 90(1):574–578, 1991.

[Sch68] Harry A. Schenck. Improved integral formulation for acoustic radiation problems. *J. Acoust. Soc. Am.*, 44(1):41–58, 1968.

[Som92] A. Sommerfeld. *Vorlesungen über theoretische Physik, Band IV: Partielle Differentialgleichungen der Physik*. Vorlesungen über theoretische Physik. Verlag Harri Deutsch, 6th edition, 1992.

[SRA08] Sascha Spors, Rudolph Rabenstein, and Jens Ahrens. The theory of wave field synthesis revisited. In *Audio Engineering Society Convention 124*, 2008.

[Teu07] Heinz Teutsch. *Modal Array Signal Processing: Principles and Applications of Acoustic Wavefield Decomposition (Lecture Notes in Control and Information Sciences)*. Springer-Verlag New York, Inc., Secaucus, NJ, USA, 2007.

[TK06] Heinz Teutsch and Walter Kellermann. Acoustic source detection and localization based on wavefield decomposition using circular microphone arrays. *The Journal of the Acoustical Society of America*, 120(5):2724–2736, 2006.

[VW04] Nicolas Valdivia and Earl G. Williams. Implicit methods of solution to integral formulations in boundary element method based nearfield acoustic holography. *The Journal of the Acoustical Society of America*, 116(3):1559–1572, 2004.

[Wei12] Eric W. Weisstein. Mathworld–a wolfram web resource, 2012.

[Wil99] E.G. Williams. *Fourier Acoustics: Sound Radiation and Nearfield Acoustical Holography*. Academic Press, 1999.

[WO02] T.W. Wu and M. Ochmann. Boundary element acoustics fundamentals and computer codes. *J. Acoust. Soc. Am.*, 111(4):1507–1508, 2002.

[Wu00] T.W. Wu. *Boundary Element Acoustics: Fundamentals and Computer Codes*. WIT, 2000.

[ZDG10] D.N. Zotkin, R. Duraiswami, and N.A. Gumerov. Plane-wave decomposition of acoustical scenes via spherical and cylindrical microphone arrays. *Audio, Speech, and Language Processing, IEEE Transactions on*, 18(1):2 –16, 2010.

[Zot09] Franz Zotter. *Analysis and Synthesis of Sound-Radiation with Spherical Arrays*. PhD thesis, University of Music and Performing Arts, Austria, 2009.

[ZPF09] Franz Zotter, Hannes Pomberger, and Matthias Frank. An alternative ambisonics formulation: Modal source strength matching and the effect of spatial aliasing. *AES 126th Convention, Munich, Germany*, 2009.

[ZT89] O.C. Zienkiewicz and R.L. Taylor. *The finite element method: Basic formulation and linear problems*. McGraw-Hill, 1989.

Fin